Differential river incision due to Quaternary faulting on the Rio Salado-Jemez system at the million-year scale

Cameron C. Reed, Karl E. Karlstrom, Ben Rodriguez, Nels A. Iverson, Matthew T. Heizler, Dylan Rose-Coss, Laura J. Crossey, Chris Cox, April Jean, Victor J. Polyak, and Yemane Asmerom, [eds.]
2024, pp. 237-256. https://doi.org/10.56577/FFC-74.237

in:

Geology of the Nacimiento Mountains and Rio Puerco Valley, Karlstrom, Karl E.;Koning, Daniel J.;Lucas, Spencer G.;Iverson, Nels A.;Crumpler, Larry S.;Aubele, Jayne C.;Blake, Johanna M.;Goff, Fraser;Kelley, Shari A., New Mexico Geological Society 74 th Annual Fall Field Conference Guidebook, 334 p.

This page is intentionally left blank to maintain order of facing pages.

New Mexico Geological Society Guidebook, 74th Fall Field Conference, 2024, p. 237–256, https://doi.org/10.56577/FFC-74.237

DIFFERENTIAL RIVER INCISION DUE TO QUATERNARY FAULTING ON THE RIO SALADO-JEMEZ SYSTEM AT THE MILLION-YEAR TIMESCALE

CAMERON C. REED[1], KARL E. KARLSTROM[1], BEN RODRIGUEZ[1], NELS A. IVERSON[2], MATTHEW T. HEIZLER[2], DYLAN ROSE-COSS[1], LAURA J. CROSSEY[1], CHRIS COX[1], APRIL JEAN[1], VICTOR J. POLYAK[1], AND YEMANE ASMEROM[1]

[1]Department of Earth and Planetary Sciences, University of New Mexico, Albuquerque, NM 871031, creed5@unm.edu
[2]New Mexico Bureau of Geology and Mineral Resources, 801 Leroy Place, Socorro, NM 87801

Abstract—Analysis of long-term average bedrock incision rates along the Rio Salado-Jemez system using fluvial terraces can be used to test and quantify the hypothesis that differential river incision reflects Quaternary fault slip during ongoing uplift of the Jemez and Nacimiento Mountains. Strath terrace flights, especially the 400–630 ka oldest straths, were correlated from the Arroyo Peñasco in the southwestern Sierra Nacimiento to the Rio Salado near the southern nose of the Nacimiento and along the Rio Jemez from San Ysidro to the Rio Guadalupe confluence and Soda Dam. By focusing on highest/oldest (400–600 ka) river terraces, resulting bedrock incision values average out ~16 glacial/interglacial cycles and are interpreted here to reflect differential uplift. For previously mapped and correlated terraces, we applied high resolution topography (HRT) datasets (1-m lidar) to refine strath heights above river level. Terrace height alone cannot be used for correlation across active faults, so we applied new and published dating based on U-series dating of travertine-cemented fluvial deposits, tephrochronology on interbedded ash, and $^{40}Ar/^{39}Ar$ dating of detrital sanidines to constrain terrace ages across the system. Significant terrace correlation uncertainties remain because of variable terrace flight preservation, need for additional age control, complexities of applying maximum/minimum age constraints, and fault geometry. Our terrace correlation working hypothesis using new geochronology suggests that Quaternary fault slip rates are similar to river incision rates, as expected in neotectonically uplifting regions. We conclude from differential incision magnitudes that uplift of the Jemez Mountains and southern Sierra Nacimiento is taking place at ~150 m/Ma relative to the Rio Grande rift and San Juan Basin over the past ~500 ka and that this surface uplift is driving some of the fastest fluvial bedrock incision rates in New Mexico at the southern nose of the Sierra Nacimiento (~300 m/Ma) and at Soda Dam on the Rio Jemez (200-250 m/Ma). Quaternary faulting is interpreted to be enhancing upthrown-side incision rates by ~100 m/Ma relative to downthrown-side bedrock incision rates of ~150 m/Ma at the confluence of the Rio Jemez and Rio Guadalupe. The proposed mechanisms driving this interaction of differential river incision and Quaternary faulting is magmatic inflation of the Jemez Mountains and related reactivation of the network of Laramide and Miocene faults around the Nacimiento-Jemez uplifts.

INTRODUCTION

The Jemez lineament is a northeast-trending zone of late Cenozoic (past ~10 Ma) dominantly basaltic volcanic fields that has been considered an important tectonic element of northern New Mexico (e.g., Aldrich, 1986; Chapin et al., 2004; Cather et al., 2012). It extends from eastern Arizona (Springerville volcanic field) along a southwest-northeast trend toward the northeast corner of New Mexico (Raton volcanic field), intersecting with the Miocene Rio Grande rift in the area of the Valles Caldera (Fig. 1). The southern margin of the lineament is collocated with a lithospheric boundary between the Proterozoic Yavapai (1.7–1.8 Ga) and Mazatzal (1.6–1.7 Ga) provinces that may have provided a path for magma to ascend to the crust during Cenozoic volcanism (Magnani et al., 2004).

The Jemez lineament has been hypothesized to be a wide zone of dynamic topographic uplift (Formento-Trigilio and Pazzaglia, 1998; Wisniewski and Pazzaglia, 2002; Karlstrom et al., 2012). Several studies (Cather et al., 2012; Nereson et al., 2013; Karlstrom et al., 2016; Repasch et al., 2017; Anderson et al., 2021) have suggested epeirogenic uplift of this wide zone over the past 10 Ma that has driven differential river incision. Cather et al. (2012) identified a broad uplift across the Jemez lineament defined by facies analysis of the Ogallala Formation in the Great Plains. Nereson et al. (2013) identified a northeast-trending zone of stream profile convexities and differential incision to support uplift of the zone relative to the Great Plains, with denudation rates of 90–114 m/Ma. Repasch et al. (2017) suggested long-term incision rates at Black Mesa and in the Taos volcanic field of 50–100 m/Ma with variations along the river due to fault-enhanced/dampened rates. Near the confluence of the Rio Chama and Rio Grande, Dethier (2001) reported an incision rate of 180 m/Ma for the 105-m terrace that contains the Lava Creek B ash; but this is the tread height, such that the bedrock incision rate for the Rio Chama is 150–160 m/Ma, using its strath height of 95–100 m and an updated LCB age of 630 ka (Jicha et al., 2016). Channer et al. (2015) reported incision rates across the Rio San José that varied from 19 m/Ma to as much as 288 m/Ma, with periods of accelerated incision from 2 to 4 Ma during construction of Mt. Taylor. The regional variations raise questions about what causes differential river incision along and across the Jemez lineament.

A key area to further test the hypothesis of differential uplift and incision is the Jemez Mountains (Fig. 1). This locality features the dynamic interaction of young volcanic systems within the Jemez lineament, Rio Grande rift faulting, and bedrock

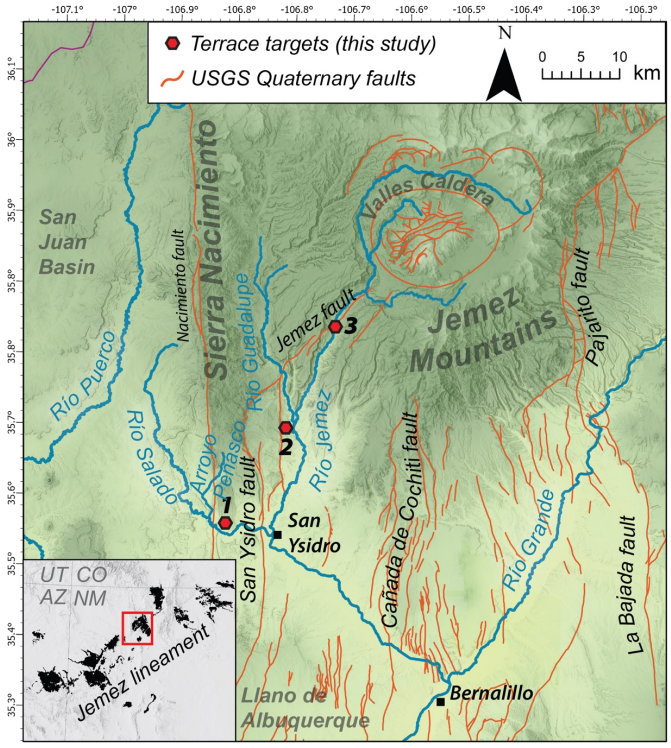

FIGURE 1. High topography of the Jemez and Sierra Nacimiento, major rivers, and faults (USGS and NMBMMR, accessed 2024, red lines). Red hexagons indicate the three high terrace localities that form the main topic of this paper: (1) Rio Salado terraces on the south plunging nose of the Sierra Nacimiento; (2) Lava Creek B-aged (630 ka) terraces near the confluence of the Rio Jemez and Rio Guadalupe; (3) Travertine-cemented gravels on the Rio Jemez at Soda Dam.

river systems draining high topography. Within our study area near the confluence of the Rio Guadalupe and Rio Jemez, Rogers (1996) reported incision rates of 120 m/Ma from 1.62 Ma (Otowi Member of Bandelier Tuff) to present and 150 m/Ma from 630 ka to present. This paper synthesizes and provides new incision rate data for three river systems that surround the southwestern side of the Jemez Mountains: Rio Jemez, Rio Salado, and Rio Puerco. We characterize the uplifted terrains, examine and compare their river profiles, and correlate and date their terraces with emphasis on the oldest/highest terraces to derive long-term rates.

METHODS

We use diverse methods in this study to measure incision rates, characterize the landscape, and synthesize datasets. Methods used here are similar to those used by other workers in correlating and dating fluvial terraces in tectonically active terranes (Wegmann and Pazzaglia, 2009; Aslan et al., 2019), tracing detrital sanidine to ignimbrite sources (Heizler et al., 2021), quantitatively analyzing river profiles (Whipple and Tucker, 1999; Wobus et al., 2006; Kirby and Whipple, 2012; Perron and Royden, 2013), parsing Quaternary fault slip by measuring differential incision across faults (Fig. 2; Pederson et al., 2002; Karlstrom et al., 2007; Crow et al., 2014), and testing for potential surface uplift driven by magmatism (Karlstrom et al., 2012).

This study targets mainly strath terraces, and reported heights are of the terrace strath—the bedrock bench carved by a paleoriver system during periods of incision and capped by bedload gravels and sands. A strath terrace tends to be thin relative to the size of the river that created it, typically less than 10 m thick (Pazzaglia, 2013). Near the confluence of the Rio Guadalupe and the Rio Jemez (La Junta), the strath terrace is buried as the basal layer of thick fill terraces and loess. Terrace formation frequently reflects alternating cycles of river incision and aggradation associated with climatic cycles (Bull, 1991; Rogers, 1996; Love and Connell, 2005; Bridgland and Westaway, 2008). Within the Rio Jemez, Rogers (1996) and Rogers and Smartt (1996) proposed a climate-driven model for incision, aggradation, and equilibrium of the Rio Jemez. In the Sierra Nacimiento, Formento-Trigilio and Pazzaglia (1998) investigated the roles of epeirogenic uplift and drainage integration, and Frankel and Pazzaglia (2006) proposed that incision was due to distant base-level fall and northward-propagating knickpoints.

Here we provide additional geochronological data for this area to evaluate terrace flights (Fig. 2) that record the past 1.6 million years of bedrock incision. This long-term analysis averages numerous glacial-interglacial cycles and can help test whether incision has been steady in a given reach, implying epeirogenic uplift (Wisniewsky and Pazzaglia, 2002; Karlstrom et al., 2012) and whether differential river incision reach-to-reach can be used to quantify Quaternary fault slip (Karlstrom et al., 2008).

Data required for incision rate studies include the height of the terrace strath above the modern bedrock strath or above river level (ARL) when the thickness of bedload gravel in the modern floodplain is unknown, and the age of the terrace strath is usually a constraining age from the overlying terrace fill or from higher or lower terraces in the same flight. Strath heights were measured accurately using 1-m lidar. New and compiled dating relied on various methods, with the most robust being the presence of a tephra that is reworked into a terrace fill such as the Yellowstone Lava Creek B ash (LCB, 630 ka; Jicha et al., 2016); this is datable using sanidine $^{40}Ar/^{39}Ar$ and/or tephrochronology (both were used in this study). U-series (U/Th) dates on travertine that cements river gravels can provide a near-direct age on gravel deposition in some instances (e.g., Crow et al., 2014) or a minimum age when veins invade older travertine or gravels (e.g., Jean et al., 2024). This is sometimes difficult to determine and is discussed case by case below. Detrital sanidine (DS) can be used on "cryptic" ashes—ash present as grains reworked into sediments—where the youngest DS grain provides a maximum depositional age (MDA; Heizler et al., 2021).

Terrace flights can yield strath-to-strath age difference to test the magnitude and variability of incision rates through the river's history (Rogers, 1996; Karlstrom et al., 2016; Aslan, 2019; Anderson et al., 2021; Crow et al., 2021; Heizler et al., 2021). Rivers flowing across faults may show relationships in which a higher rate of bedrock incision in upthrown blocks equals the incision rate on the downthrown block plus the fault

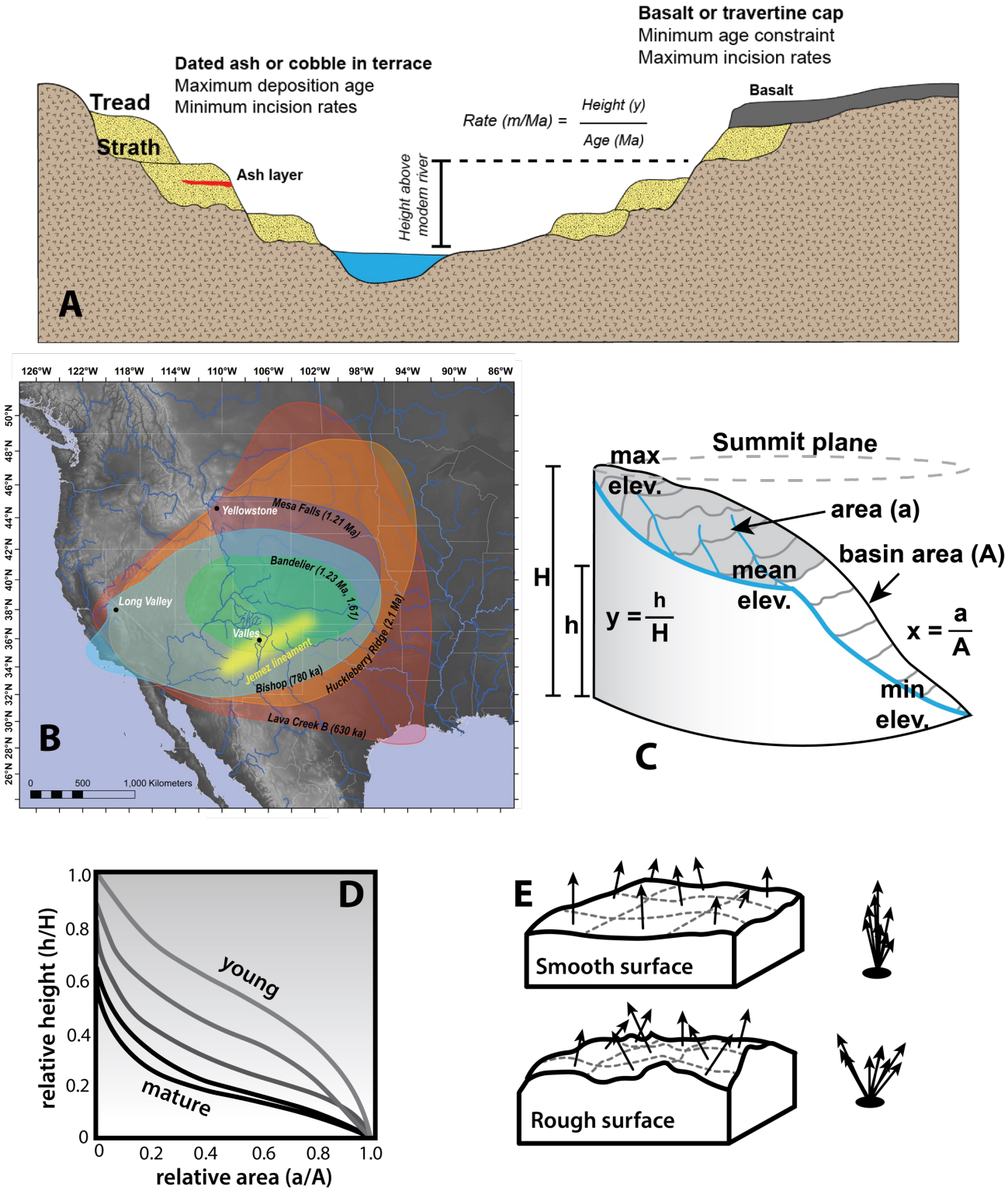

FIGURE 2. (A) Sketch of a generalized river terrace flight with the presence of multiple chronometers and strath terraces. For this study, geomorphic terrace nomenclature and correlation was from Rogers and Smartt (1996), Formento-Trigilio (1997), Pazzaglia et al. (1997), Formento-Trigilio and Pazzaglia (1998), Formento-Trigilio et al. (1998), and Kelley et al. (2023). (B) Tephrochronology was used to correlate glass compositions to known Lava Creek B (red line, 630 ka per Jicha et al., 2016) tephra compositions; other techniques for age control include detrital sanidine analyses and U-series dating. (C) Parameters utilized for calculating elevation-relief ratio and the hypsometric integral within a drainage (Pike and Wilson, 1971; modified after Ritter et al., 2002). (D) Terrain analysis involved hypsometric integral (HI) (Jaiswara et al. 2020 after Ohmori 1993), and (E) roughness analysis showing surface unit vectors that have similar orientations in smooth terrain and variable vectors in rough terrain, roughness calculated by the terrain ruggedness index of Riley et al. (1999) that calculates difference in elevation between cells in a moving window (figure from Hobson, 1972 modified).

slip rate (Howard et al., 1994; Whipple and Tucker, 1999; Pederson et al., 2002; Tucker and Whipple, 2002; Karlstrom et al., 2007, 2008; Whittaker et al., 2008; Crow et al., 2014; Repasch et al., 2017). This method allows for the determination of the magnitude of slip across faults, including those with low rates on the margins of the Colorado Plateau and Rio Grande Rift (e.g., Thompson Jobe and Chupik, 2021).

High-Resolution Topographic Data and River Profile Analysis

Quantitative parameters used to investigate erosion of landscapes by bedrock rivers include chi (χ) and k_{sn} steepness indices (Howard 1994; Whipple and Tucker 1999), which may help reveal disequilibrium within a stream that can cause variable incision rates, for example, variations due to knickpoint migration, rock-type erodibility differences, or differential uplift. The normalized steepness index (k_{sn}) is quantified using a power law relationship between channel gradient (S) and the upstream drainage area (A) given the reference concavity (θ_n, often 0.45; Flint, 1974; Kirby and Whipple, 2012), as described by Equation 1 (Kirby and Whipple, 2012):

$$S = k_{sn}A^{-\theta}$$

When in steady state, the erosion rate of a stream is equal to the rock uplift rate ($E = U$), whereby K is the erosional efficiency factor that accounts for lithology, climate, channel geometry, and sediment supply (Howard et al., 1994; Whipple and Tucker, 1999), and the m/n ratio represents stream power per unit area or other channel dynamics (Tucker and Whipple, 2002), as demonstrated by Equation 2 (Sklar and Dietrich, 1998):

$$S_e = \left(\frac{U}{K}\right)^{\frac{1}{n}} A^{\frac{-m}{n}}$$

χ (chi) is the integral of the reference drainage area (Ao) divided by the relative drainage area (the area above a given upstream distance, Ax) raised to the exponent of the m/n ratio, as given in Equation 3 (Perron and Royden, 2013):

Chi is used to examine the influence of rock uplift rate and

$$\chi = \int_{xb}^{x} \left(\frac{A_0}{A(x)}\right)^{\frac{m}{n}} dx$$

erodibility (U and K) across different stream profiles even if their profiles are not in steady state and if U and K are spatially variable.

χ disequilibria across basin divides indicates a migration of the divide from lower to higher χ values unless maintained by differences in lithology or uplift (Willett et al., 2014). χ analysis of the Rio Salado and Rio Puerco basins provides information to determine whether any significant transient Quaternary disturbance exists along divides of the basins and will help identify whether the Rio Salado-Jemez system is in equilibrium or actively adjusting, for example to bedrock variations, geomorphic forcings like stream capture, or tectonic forcings like differential uplift.

Simple morphometric tools to evaluate landscape maturity and evolution include the hypsometric integral (HI) and roughness. To demonstrate the HI, a schematic drainage basin is presented in Figure 2C. In this figure, H is the total vertical relief in the basin; total surface area of the basin is represented by A, while area (a) is the surface area above a given elevation (h). The hypsometric curve plots the relative drainage area of a basin above a relative elevation and represents the cumulative frequency distribution of elevations within the landscape (examples of different curves that reflect different-aged landscapes are shown in Fig. 2D). The hypsometric integral is the area below the hypsometric curve (Strahler, 1952; Fig. 2C and 2D) and is identical to the elevation-relief ratio (Pike and Wilson, 1971). The elevation relief ratio is defined as mean elevation minus minimum elevation divided by relief and is calculated in a moving window of a defined radius (Pike and Wilson, 1971). Landscapes that have reached maturity generally have lower HI and concave-up hypsometric curves, while youthful landscapes have higher HI and hypsometric convex-up curves (Strahler, 1952). By plotting the HI value of a moving window, it is easier to visualize areas consistent with young relief versus areas of preserved stability. Roughness, or the ruggedness index, quantifies the mean absolute difference in elevation from one cell to the next (Fig. 2E) and can clearly display young geomorphic features like scarps and offsets better than a traditional hillshade.

TopoToolbox, a MATLAB-based plug-in software for geomorphic modeling (Schwanghart and Scherler, 2014), was used to conduct these analyses. A 10-m DEM of the study region was used rather than 1-m lidar to allow more efficient processing with similar results for k_{sn} analysis (Purinton and Bookhagen, 2017). Analysis of roughness and hypsometric integral (HI) were completed using TopoToolbox with a 1000-cell (10-m) radius moving window. Ruggedness was calculated according to the topographic ruggedness index (Riley et al., 1999) in TopoToolbox from a 10-m DEM. χ analysis was done using ChiProfiler (Gallen and Wegmann, 2017) that utilizes TopoToolbox in the Matlab environment.

RESULTS

Terrain Analysis

Figure 3A shows the hypsometric integral from the elevation-relief ratio (per Pike and Wilson, 1971), processed for the landscape around the Jemez Mountains and Sierra Nacimiento from a 10-m DEM. This evaluates the relative development stage of topography (Strahler, 1952; Ohmori, 1993; Jaiswara et al., 2020). Low values represent extensive level surface with isolated relief features, like floodplains, whereas high values can reflect broad, level surface broken by depressions or incised features (Pike and Wilson, 1971; Fig. 3A). The elevation-relief ratio of the area surrounding the Jemez Mountains and the Sierra Nacimiento may demonstrate the relative youthfulness of the high topography in contrast to the well-adjusted and incised front of the Sierra Nacimiento and Rio Jemez floodplain.

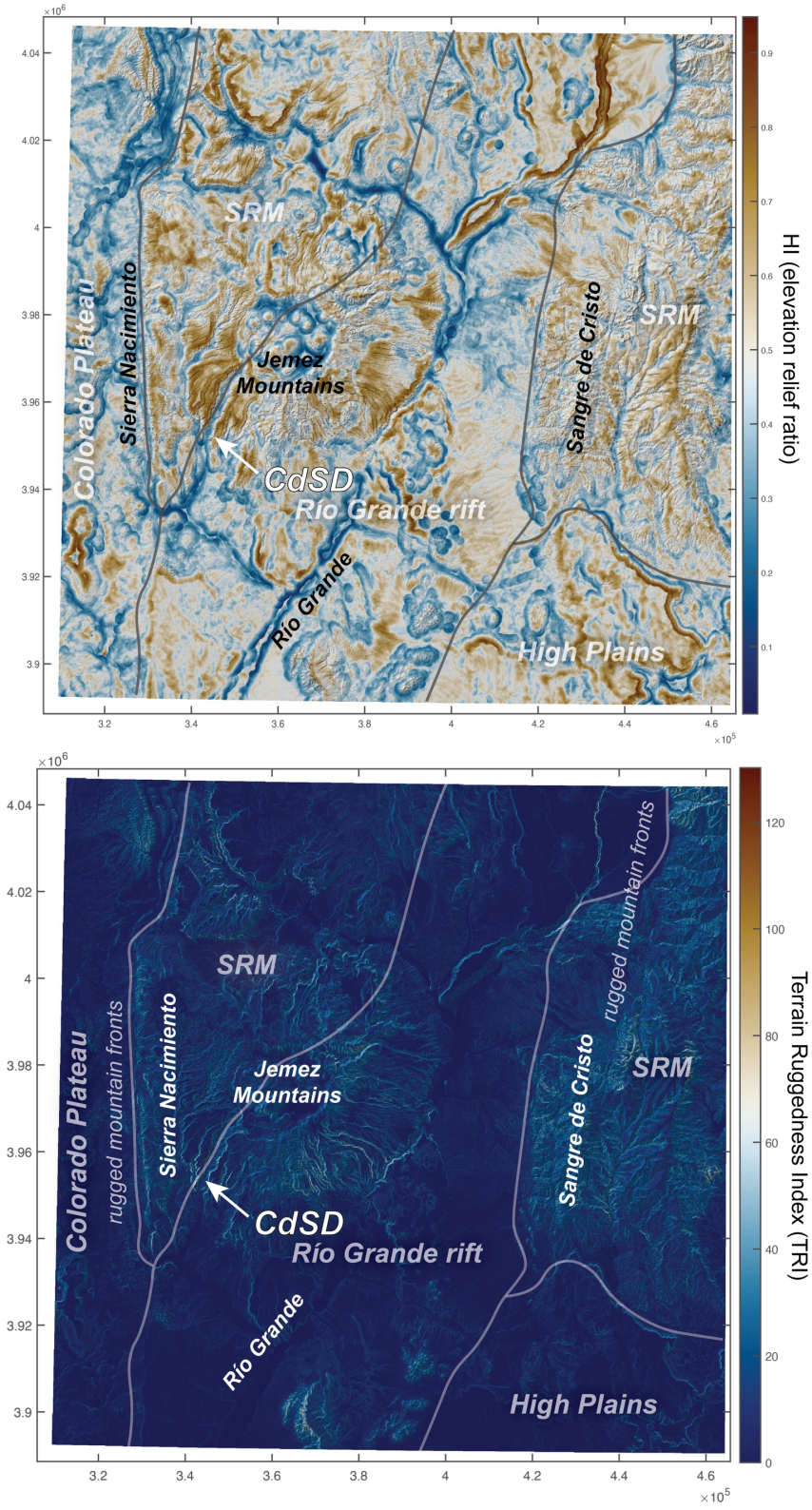

FIGURE 3. Terrain analysis. (A) Hypsometric integral (HI) map, calculated using the elevation-relief ratio method of Pike and Wilson (1971), shows the extent of broad high topography incised by narrow canyons in the combined Jemez-Nacimiento uplifts. The Jemez-Nacimiento uplift hypsometry is filtered through a 200 cell (10m) radius moving window and is consistent with relative youthfulness of the mountains due to uplift and emplacement of the 1.6 and 1.2 Ma, >100 m thick Bandelier tuffs related to Jemez Mountains volcanism. (B) Roughness map shows high roughness in what we interpret to be neotectonically uplifting topography. The similar dimensions and geomorphic states of the Quaternary Jemez Mountains and the Laramide Sierra Nacimiento suggests the possibility that Quaternary and ongoing uplift of the Jemez Mountains is driving renewed uplift of the southern Sierra Nacimiento. Elevated roughness gradients in the Sangre de Cristo clearly trend across mountain front faults and harder lithologies. CdSD is San Diego Canyon.

The Sierra Nacimiento and Jemez Mountains in this view are difficult to decouple and have similar north-south dimensions of high and incised topography, raising the possibility that both are responding to a Quaternary landscape perturbation caused by volcanism (e.g., deposition of >100 m of Bandelier Tuff) and the cumulative surface uplift of the Jemez Mountains due to volcano construction plus potential epeirogenic uplift.

In roughness (Fig. 3B), the Jemez Mountains and Sierra Nacimiento are both rugged landscapes relative to the San Juan Basin to the west and the Rio Grande rift to the southeast. The roughness map (Fig. 3B) is similar to Figure 3A in highlighting major tectonic features, such as the 80-km-long Sierra Nacimiento uplift bounded by the Nacimiento fault zone and the closely corresponding elevation, diameter, and roughness between the Sierra Nacimiento and Jemez Mountains. Incised features such as Cañon de San Diego (CdSD in Fig. 4) are clear in both images, reflecting rapid Quaternary incision that is leaving high topography stranded.

χ values (Fig. 4A) and k_{sn} (Fig. 4B) of the Rio Jemez basin and adjacent rivers show over-steepened reaches caused by lithologic and tectonic controls. χ, a measure of basin divide stability, can assess basin-level rather than stream-level disequilibrium (Willett et al., 2014). χ analysis (Fig. 4A) reveals significant disequilibrium across two divides: Rio Puerco-Rio Salado and Arroyo Peñasco-Rio Salado. The Arroyo Peñasco-Rio Salado basin has higher χ than neighboring basins, suggesting that lithology and/or tectonic controls are maintaining high χ values across the southern nose of the Sierra Nacimiento. This analysis may also reflect the capture of the Arroyo Peñasco by the Rio Salado that was interpreted to be due to erosional variability of lithology (Formento-Trigilio and Pazzaglia, 1998).

Within the k_{sn} map, steeper normalized channel gradients are collocated with major faults and lithologic changes (Figs. 4B and 5). The relatively low k_{sn} of the Rio Guadalupe and Rio Jemez at La Junta (LJ of Fig. 4B) supports that the two rivers are currently at a state of relative equilibrium (Rogers, 1996). Notable areas with elevated k_{sn} include reaches of the Rio Guadalupe (e.g., the Guadalupe box [GB] in Fig. 4B) and the Rio Jemez upstream from La Junta (Fig. 4B). Additionally, tributary streams that cross the San Ysidro-Jemez fault zone have higher k_{sn} on the upthrown side of the fault. Some faults have uplifted, resistant basement rocks, leading to over-steepened reaches and making it difficult to parse lithologic versus tectonic controls, as across the Nacimiento front and Guadalupe box (GB and NF of Fig. 4B), where lithology likely contrib-

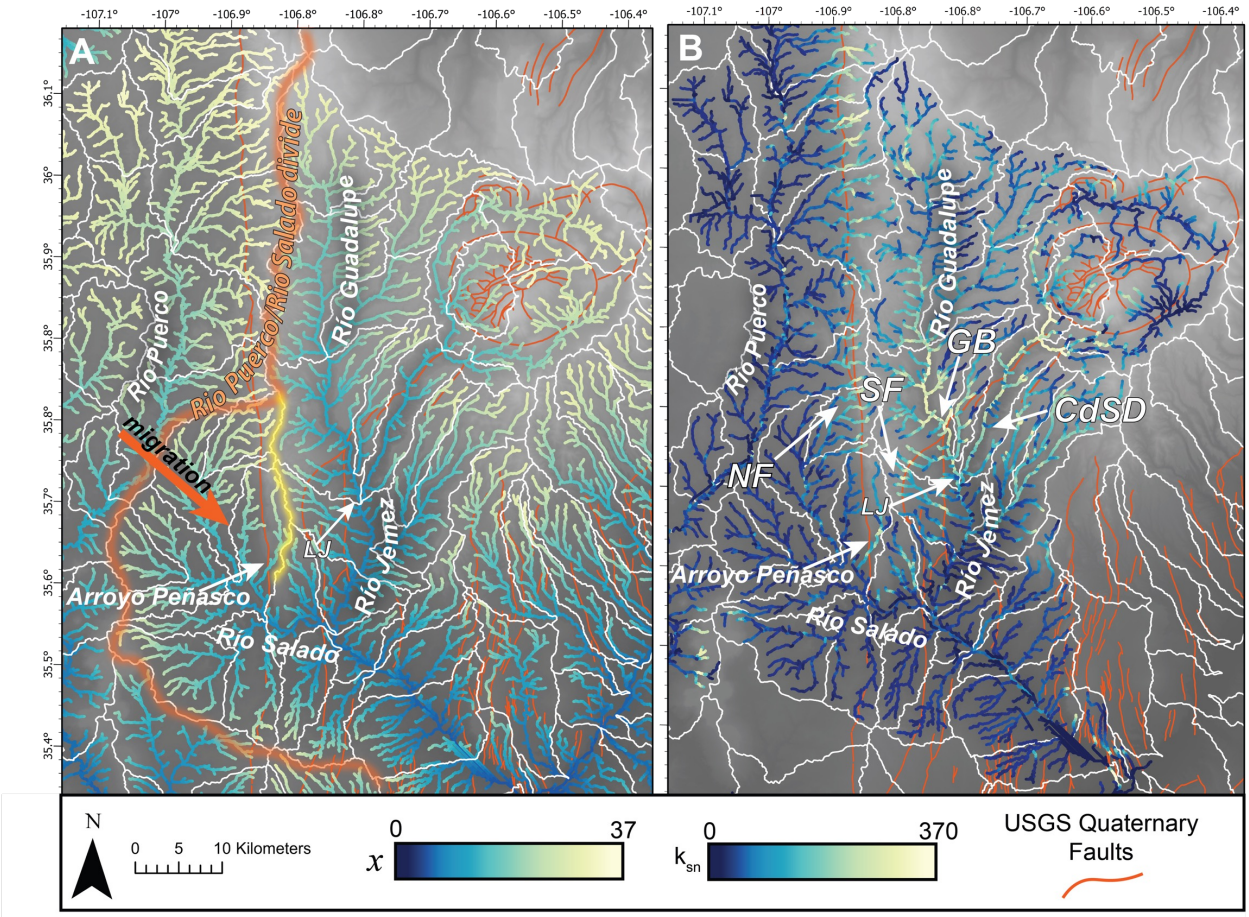

FIGURE 4. (A) χ analysis shows divide instabilities between the Rio Puerco and Rio Salado, with higher χ in the Rio Salado than the Rio Puerco that favors divide migration into the Rio Salado drainage. (B) k_{sn} analysis of normalized river steepness from 10 m DEM shows over-steepened reaches in the Precambrian basement of the Sierra Nacimiento and Nacimiento fault (NF), in the Rio Jemez of Cañon de San Diego (CdSD), in the Rio Guadalupe and Guadalupe box (GB), and across some faults. Major basin divides are colored, minor basin divides are shown in white (USGS, 2019). GB = Guadalupe Box, LJ = confluence of the Rio Guadalupe with the Rio Jemez at La Junta, NF = Nacimiento fault, SF = Sierrita fault. Quaternary faults are shown in red (USGS and NMBGMR, accessed 2024).

utes to steepness. Other areas of high k_{sn} may reflect faults and fault-related knickpoints, such as the over-steepened reaches draining the southeastern Sierra Nacimiento, as demonstrated in Figure 5.

Examination of the k_{sn} analysis of tributary streams in the southern Sierra Nacimiento (Fig. 5A) reveals that elevated k_{sn} values are concentrated upstream of major fault segments, suggesting a response to young movement across the faults. Two regions of interest are where tributary streams cross normal faults. Rock strength and hardness are classified by color according to Cikoski and Koning (2017) to account for generalized lithologic influences on steepness. Figure 5B shows tributaries draining the eastern slopes of the Sierra Nacimiento to the Rio Jemez and crossing the Sierrita fault, the arching north-

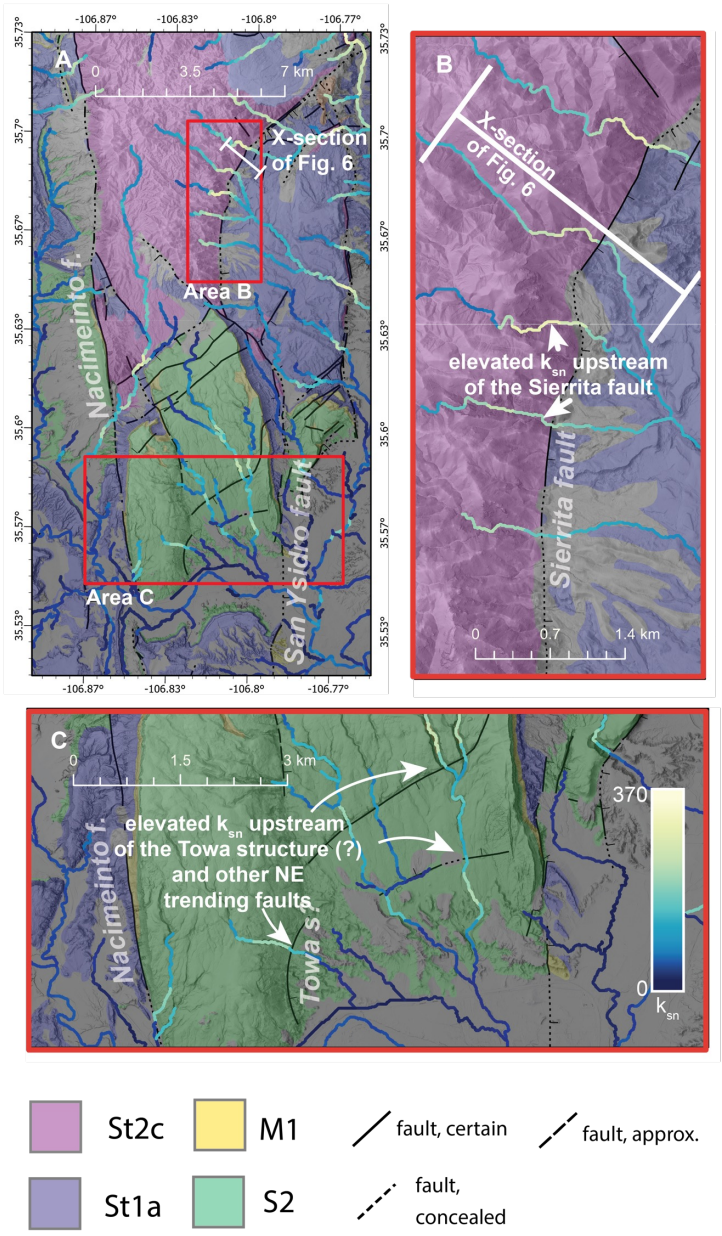

FIGURE 5. Detailed k_{sn} maps of tributary drainages in the southern Sierra Nacimiento. (A) Index for large scale maps of eastern slope of the southern Sierra Nacimiento (B) and the southernmost Sierra Nacimiento (C). Note that the stream color shades relate to k_{sn} (as shown in C) and the map-area shades correspond to lithology (key at bottom of figure). Map colors correspond to generalized landslide units of Cikoski and Koning (2017), which reflect lithologic characteristics germane to landslide susceptibility (generalized rock hardness vs. softness or interbedding of hard vs. soft lithologies). In increasing magnitude of relative hardness, the units are categorized as: S2 (green, weak sedimentary rocks that are well consolidated and mostly cemented; this includes both the Chinle Group and the harder Agua Zarca Sandstone), M1 (yellow, interbedded weak and strong sedimentary rocks, assumed moderate strength), St1a (indigo, hard caprock underlain by softer sedimentary rocks), St2c (pink, thick Proterozoic rocks). Brown, unlabeled shades is soft Quaternary alluvium and Santa FE Group sediment. We use an informal term, Towa structure, to tentatively link: (1) partially reactivated east-up monocline south of Highway 550 (Kelley, 1977), linear east-down ramp that hosts travertine-depositing springs, and east-down and southeast-down faults mapped by Woodward and Reutschilling (1976) and Kelley (1977). The harder Agua Zarca Formation is found west of the black line drawn for the Towa structure and the softer Petrified Forest is found on the east. These structures are collocated with tributaries showing high normalized steepness at and upstream of the fault. (B) Tributaries crossing the Sierrita (down to the east) also exhibit steeper reaches at and upstream (west) of the fault with the location of Figure 6A shown. (C) Blow up of Rio Salado tributaries shows the same response to faults and lithologic differences.

east-trending segment that connects the San Ysidro and Jemez faults within the San Ysidro-Jemez fault system (Karlstrom et al., 2024). These show elevated k_{sn} upstream of multiple faults then a return to near equilibrium gradient farther upstream, all in the same generalized map unit. Figure 5C shows streams that cross an informally named Towa structure and show a similar pattern across multiple faults, all within Permian strata. The Permian section consists of hard Agua Zarca Formation overlain by erodible Petrified Forest Formation; some k_{sn} differences in Figure 5C correspond to those lithologic changes, but other k_{sn} changes occur in the same formation (cf. Woodward and Ruetschilling, 1978) of uniform hardness, which only in part reflects the contrast between basal Agua Zarca Sandstone and the weaker Petrified Forest Formation. These patterns suggest that neotectonic movement across faults is an important control on these tributary gradients that can be enhanced when Precambrian bedrock is brought up on the faults, such as at the Sierrita fault of Figure 5B.

The observed steepened reaches and knickpoints of tributary streams (high k_{sn}) provide evidence of a neotectonically active landscape in the southern Sierra Nacimiento across major fault segments. Figure 6A demonstrates a conceptualized block diagram of tributary streams crossing a normal fault (like the Sierrita), with k_{sn} patterns shown as the color gradient. Where the normal fault brings up harder basement rock in the footwall, an additional lithologic control is contributed and superimposed on knickpoint formation (Wobus et al., 2006). Figure 6B shows a time series as the knickpoint widens and migrates upstream. Terraces are offset, and differential heights relative to the steepened profile reflect fault slip. Thus, for the Sierrita fault and the east-northeast-striking faults on the southeastern end of the Nacimiento Mountains, we interpret k_{sn} data to indicate tributaries that are adjusting to Quaternary faulting.

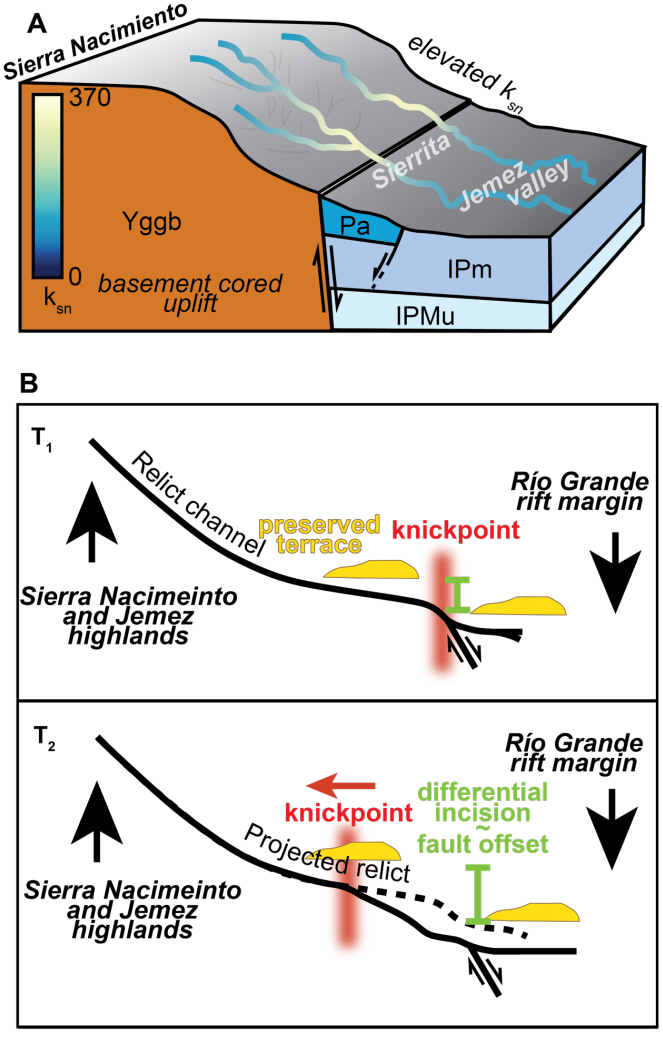

FIGURE 6. (A) Simplified block diagram with the basement-cored uplift of the Sierra Nacimiento and the Sierrita normal fault. Tributary streams have steeper reaches at and just upstream of the fault (high k_{sn} values that may correspond to knickpoints) but return to lower-sloping, concave-up (equilibrium) profiles (low k_{sn} values) upstream. (B) Time series diagrams of stream profiles provide an explanation for observed steepness: knickpoints collocated at faults are transient responses to fault movement; the knickpoint propagates upstream as the channel responds to the change. The offset can be measured by offset on preserved terraces, primarily on mainstem streams. Time series adapted from Armstrong et al. (2021).

River Terrace Correlations

Figure 7 shows our river terrace correlations along the Rio Salado-Jemez system. The Rio Salado drains the western Sierra Nacimiento and joins the Rio Jemez that drains the Jemez Mountains to form a major tributary to the Rio Grande. Because of the numerous faults that cross the rivers, we divide the terraces into fault-bounded subareas, within which flights of terraces have not been significantly modified by faulting (subareas 1–6 of Fig. 7). These terraces have been traced and correlated by several workers within these areas (e.g., Rogers, 1996; Rogers and Smartt, 1996) and between these areas (Formento-Trigilio and Pazzaglia, 1998; Tafoya, 2012; Kelley et al., 2023), but ours is the first attempt to integrate all six areas including the newly dated terrace flight on the southern nose of the Sierra Nacimiento. The terrace flight subareas include the southwest flank of the Sierra Nacimiento (subarea 1), the south-plunging nose of the Nacimiento uplift (subarea 2), the Rio Salado-Jemez confluence near San Ysidro (subarea 3), the lower Rio Jemez near Cañon and Walatowa (subarea 4), the Soda Dam area (subarea 5), and near Zia Pueblo (subarea 6). Formento-Trigilio and Pazzaglia (1998) and Formento-Trigilio et al. (1998) correlated terraces across subareas 1, 3, 4, 5, and 6, but we add new geochronology and refined heights from 1-m lidar. Rogers and Smart (1996) and Rogers (1996) worked in subarea 4 and calibrated long-term rates with a key terrace that contains the Lava Creek B ash (630 ka). For subareas 2 and 5, we present new terrace characterization and age constraints from U-series and DS geochronology. These data significantly change the terrace correlation of Frankel and Pazzaglia (2006, fig. 8) between subareas 4 and 5.

Terrace Heights and Ages

Figures 7 and 8 summarize height and age information for key terraces from each subarea. These refined heights and ages can be used to test the correlation of Formento-Trigilio and Pazzaglia (1998), essentially followed by Kelley et al. (2023),

who named and correlated Qt1 and Qt2—the highest and second-highest mapped Quaternary terraces within each flight—as well as lower terraces Qt3 to Qt6 leading down to the active flood plain. Formento-Trigilio and Pazzaglia (1998) proposed a fault-influenced incision model and identified several Quaternary faults based on terrace offsets. The next section below tests this correlation with focus on the higher terraces in subareas 2, 4, and 5, where our geochronology data show lower incision rates in subarea 4 than in subareas 2 and 5 over the past ~500 ka. The published correlations combined with our preferred ages for subarea 5 would necessitate large offset across the Towa structure. We also explore alternative terrace correlations that partition this differential incision across other faults.

A terrace flight at Rio Salado (subarea 2) on the south-plunging nose of the Sierra Nacimiento is newly described and dated in this paper and provides a potential template for terrace correlation. Eight thin (a few meters thick) terraces of river cobbles and sands rest on a thin skin of the Petrified Forest Member of the Chinle Formation preserved on the Agua Zarca dip slope, and many are capped by travertines (Fig. 9). Although U-series ages of travertine are minimum ages, we assume that travertine deposition closely followed strath and floodplain development, perhaps within several to 10 ka and within the error of the U-series dates. This assumption is based on the semi-regular ~100 ka scale of increasing age upward in the terrace flight, the analogy to the modern river where modern ojitos are depositing travertine mounds atop Rio Salado alluvium in the modern floodplain, and the apparent role of travertine deposits in preserving both the thin skin of Petrified Forest Member and the thin gravels on the Agua Zarca dip slope. U/Th dates on samples of travertines capping Rio Salado gravels are shown in Figure 9A and listed in Table 1. The highest terraces (Qt1a and 1b) are 195 m and 164 m ARL; ages are beyond U-series range (>500 ka), but Qt1b gives a ^{238}U model age of 534±148 ka. We tentatively correlate Qt1 to here based on relative height differences of Qt1 and Qt2 elsewhere (~20–40 m; Fig. 8), which is allowable by the Qt1b model age. The next highest terrace (Qt2) is 130 m ARL and gives a U-series date of 415±16 ka. Qt4 is 44 m ARL and gives a U-series age of 250 ka. ^{40}Ar/^{39}Ar DS samples were collected from terrace fill beneath several of the dated travertines with youngest grains of ~1.2 Ma; these provide maximum age constraints that are compatible with the U-series dates. They do not help to further refine the strath ages (Table 1), but they do provide provenance data for the terraces and show that the 250 ka 44 m terrace has similarity to the <261 ka San Ysidro surface that may be graded to it (Bailey et al., 2024).

Subarea 3 (Fig. 8) is on the Rio Salado and contains the San Ysidro terraces. Formento-Trigilio (1997), Formento-Trigilio et al. (1998), and Formento-Trigilio and Pazzaglia (1998) correlated Qt2 (55 m) in this area to the Qt2 (45m) in subarea 4, where they estimated an age of 400±100 ka based on soil development. This age is similar to the 415±16 ka U-series-dated travertine of Qt2 (130 m) in subarea 2. If this published correlation is correct (our Alternative 1), there is a 75-m height difference in the ~400 ka terraces between subareas 2 and 3 that could be explained by 75 m of east-down displacement across the Towa structure in the past 400 ka. The base of the Petrified Forest Formation is an east-down ramp or monocline with about 100 m of vertical separation, but there is no obvious fault plane or scarp. An alternative (Alternative 2) would be to correlate Qt2 and Qt4 in subarea 3 with the 250 ka Qt4 in subarea 2. In this alternative correlation, there need be no Quaternary displacement across the Towa structure, and instead, the required 60 m offset of Qt2 between subareas 2 and 4 (Fig. 8) may have taken place on the San Ysidro fault.

Subarea 4 is on the Rio Jemez and extends from Walatowa to the Rio Jemez-Rio Guadalupe confluence at La Junta. It has a well-developed terrace flight on the west side of the river and less-well-preserved paired terraces on the east. The highest terraces at La Junta (Fig. 10) are an important keystone that provides an age for Qt1 because it has the 630 ka (Jicha et al., 2016) Lava Creek B (LCB) Yellowstone ash in it (Rogers, 1996; Rogers and Smartt, 1996). The Qt1 terrace (Fig. 10A) is a fill terrace that sits on a well-preserved strath developed on Permian sediments (Abo Formation) and consists of 22 m of sediment (~3–4 m of cemented river cobbles with sparse fine sand lenses overlain by 11 m of sands, silts, and fine gravels overlain by 7 m of coarse gravel; Rogers and Smartt, 1996, fig. 5). A prominent 1–2-m-thick ash-rich layer sits 5 m above the strath and is capped by about 17 m more alluvium and terrace deposits.

We resampled the terrace and ash in several places for ^{40}Ar/^{39}Ar dating to confirm the presence of 630 ka Lava Creek B ash. We sampled at the strath within a sand lens (CR22-G1), the basal part of the ash layer (CR22-G2), and the terrace material above the ash layer (CR22-G3). ^{40}Ar/^{39}Ar dating (Fig. 10B) for all three samples returned bimodal weighted MDAs with a prominent peak at 1.22 Ma (Upper Bandelier Tuff, UBT) and one centered at 604±15 ka, the latter comprising exclusively grains from sample CR22-G2 (the ash sample). The oldest normal distribution of the youngest grains provided a date of 633±10 ka (Fig. 10B). The older age closely matches the known age of the LCB eruption (630 ka; Jicha et al., 2016) compared to the youngest normal distribution of 533±16 ka, which may be explained by ^{40}Ar loss. We also processed volcanic glass samples for microprobe tephrochronology to determine agreement with the microprobe analysis of Rogers (1996) given the alternate possibility that such a well-preserved ash may be from the nearby Valles Caldera. Results confirmed a match in tephra chemistry (CaO versus FeO) of the CR22-G2 sample (Fig. 10C, black dots) with that of LCB (red circles; Perkins et al., 1995) and not with the Tshirege Member of the Bandelier Tuff or ash-fall units of the Pajarito plateau (WoldeGabriel et al., 2007). Our results agree with Rogers (1996) and provide additional geochronology for this ash. Using a strath height of 90 m for Qt1 in subarea 4, we calculate an average bedrock incision rate of 143 m/Ma since 0.63 Ma. Rogers (1996) cited an incision rate of ~150 m/Ma using the tread height of 111 m (rather than the 90 m strath height) and an LCB age of 620 ka (rather than 630 ka).

For Qt2 in subarea 4, Rogers (1996) estimated an age of 500 ka using a combination of stratigraphic position, amino acid racemization ratios, incision rates, correlation with dated terraces

of the Rio Chama, and an attempt to correlate terrace formation with the glacial and interglacial oscillations calibrated by the marine isotope stage (MIS) curve. This estimated age is approximately compatible with our 415 ka age from subarea 2.

Figure 8 shows Qt1 in subarea 2 as 164 m ARL, 534 ka, yielding an incision rate of 307 m/Ma and Qt2 as 130m ARL, 415 ka, yielding an incision rate of 313 m/Ma. Near La Junta (subarea 4), the Qt1 strath is 90 m ARL, and we use the Lava Creek B ash age of 630 ka, yielding a lower incision rate of 143 m/Ma. This rate is consistent with the incision rate of 175 m/Ma for Qt2 using 70 m ARL and 400 ka. The difference in incision rates between subarea 2 (~310 m/Ma) and subarea 4 (~140 m/Ma) is 170 m/Ma, hence 85 m over the past 500 ka. The height difference of 74 m for Qt1 and 60 m for Qt2 for

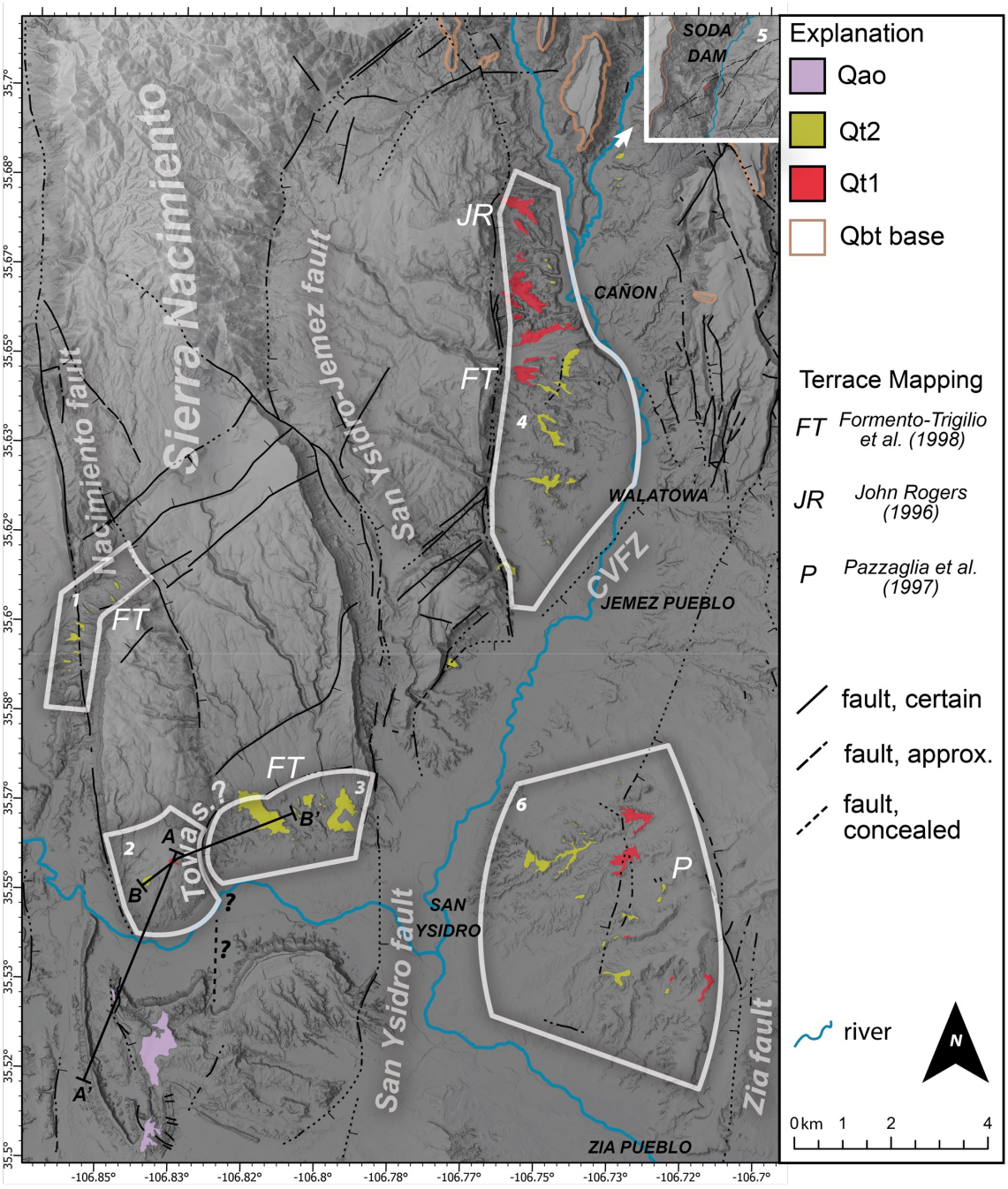

FIGURE 7. Six subareas areas where terrace flights are correlated by height, age, and fill/tread/soil character. Qao is Quaternary aeolian + alluvial deposits that cap the beveled surfaces across the Tierra Amarilla anticline, Qt2 is the second highest terrace correlated across the Rio Salado and Rio Jemez; Qt1 is the highest correlated terrace of the Rio Salado and Rio Jemez system (Formento-Trigilio and Pazzaglia, 1998; Formento-Trigilio et al., 1998; Kelley et al., 2023). Subareas are: (1) **Arroyo Peñasco**: terraces commonly overlain by travertine-cemented platforms; (2) **Rio Salado**: the southern nose of the Sierra Nacimiento has gravel terraces cemented by travertine, which was dated using U-series methods; (3) **San Ysidro**: Rio Salado terraces located 2–4 km west of San Ysidro; (4) **Walatowa** (south) and **La Junta** (north): Rio Jemez terraces at Walatowa and La Junta near the Jemez-Guadalupe confluence, where Qt1 contains the Lava Creek B ash (630 ka; Jicha et al., 2016); (5) **Soda Dam:** U-series dated travertine-cemented gravels at Soda Dam on a structural horst within the Jemez fault zone; (6) **Zia Pueblo:** Located 1–6 km east of San Ysidro, these terraces may contain past paleoconfluence locations of Rio Salado and Rio Jemez.

age-correlative terraces between subareas 2 and 4 is attributed to differential incision due to faulting. With Alternative 1, correlating terraces between subareas 2 and 3 results in 74 m of vertical displacement across the Towa structure. The Alternative 2 correlation between the two subareas (i.e., correlate Qt2 and Qt4 in subarea 3 with the 250 ka Qt4 in subarea 2), results in zero displacement across the Towa structure and up to 60–70 m of vertical displacement on the San Ysidro-Jemez fault (the 60–70 m is obtained from comparison of the Qt1 and Qt2 heights in subareas 4 and 6, east of the fault, with Qt1 and Qt2 heights in subarea 3, west of the fault). The resulting vertical offset value of 60–70 m is higher than the 6–11 m of post-630 ka vertical offset interpreted on the San Ysidro fault by Formento-Trigilio and Pazzaglia (1996) and Formento-Trigilio (1997). The calculated slip rate for using the alternative correlation results in a vertical slip rate of ~100 m/Ma, which is compatible with a Late Quaternary slip rate of <200 m/Ma for the San Ysidro fault (Kelson et al., 2015) and higher than the 27–54 m/Ma interpreted for its southern extension, the Calabacillas fault (McCalpin, 2011).

	Terrace Group	Heights ARL (m)	Ages (ka)	Incision Rates (m/Ma)	Fault	Est. slip (m) (terrace used)
1	Arroyo Peñasco	Qt2: 80m	none* Qt2: 415 [1]	193*		
2	Río Salado	Qt1: 164 m Qt2: 130 m Qt4: 44 m	Qt1: 534 ± 148 [2] Qt2: 415 ± 16 [3] Qt4: 250 ± 4 [4]	Qt1: 307 Qt2: 313 Qt4: 176	Nacimiento fault	<50 (Qt2)
3	San Ysidro	Qt2: 45m Qt4: 45m	Qt2: 400 ± 100 [5] Qt4: 250 ± 4 [4]	Qt2: 113 Qt4: 180	Towa structure	<85 (Qt2) ~0 (Qt4)
4	Walatowa	Qt1: 110m Qt2: 70m Qt4: 30m	Qt1: 631 ± 1 [6] Qt2: 415 ± 16 - 500 [7]	Qt1: 174 Qt2: 169	San Ysidro + CVFZ	25 (Qt2) 15 (Qt4)
	La Junta	Qt1: 90m Qt2: 70m Qg3: 185m	Qg3: 1.23 Ma [8]	Qt1: 143 Qt2: 169 Qg3: 150		
5	Soda Dam	Qt1: 150m Qbt: 385m	Qt1: 560 ± 323 [9] Qbt: 1.62 Ma [10]	Qt1: 268 Qbt: 238	Jemez fault	60 (Qt1)
3	San Ysidro	Qt2: 45m Qt4: 45m	Qt2: 400 ± 100 [5] Qt4: 259 ± 3 [4]	Qt2: 113 Qt4: 174	San Ysidro fault	15 (Qt2) 11 (Qt4)
6	Zia	Qt1: 100 m Qt2: 60-65m Qt4: 34 m	Qt1: 631 ± 1 [11] Qt2: 400 ± 100 [12] Qt4: 259 ± 3 [4]	Qt1: 160 Qt2: 150 Qt4: 130		

FIGURE 8. Summary table and index map of terrace ages, heights, and incision rates for each terrace subarea (1-6) using our preferred correlation and assumption that U-series ages are close to depositional ages (alternative 1). Differences in incision rates between subareas are attributed to post-630 ka fault slip (rightmost column) on the fault segments shown. Arrows on faults indicate relative movement (east or west side down) as if in cross sectional view from the south. Longer-term bedrock incision (canyon deepening) rates are shown from the base of the lower Bandelier where available (see text for complexities). Differential incision is calculated between available correlated terraces, either Qt1 or Qt2, and assumes the high terraces at Soda Dam and Sierra Nacimiento may correlate to the 630 ka Lava Creek B terrace, which is permitted but not dictated by the geochronologic data. For subarea 3, the red text reflects the 45 m ARL terrace being Qt2 (alternative 1) and green text reflects the 45 m ARL being Qt4 of Formento-Trigilio et al. (1998) and Formento-Trigilio and Pazzaglia, (1996) (alternative 2) correlations. Footnotes (superscript numerals in Ages column): are as follows: (1) Formento-Trigilio et al. (1998) correlate these surfaces to the Qt2 terraces on the Rio Jemez, where proposed ages include 310 ± 70 ka to 425 ka (Rogers, 1996; Rogers and Smartt, 1996) and a 400±100 ka estimate from soil development (Formento-Trigilio and Pazzaglia, 1998). These agree with the 415 ± 16 ka U-series age from travertine in a 130 m ARL terrace at Rio Salado (subarea 2). (2) U-series model age on travertine caps on highest terraces from Cron et al (2024). The high Qt1 terrace on the Rio Salado is beyond U-series dating range but have a 238U model age of 534 ± 148 ka; Qt2 is 415 ± 16 ka. (3) U-series age on travertine caps on second highest terraces from Cron et al (2024). (4) U-series age on travertine caps on 44m ARL terrace from Cron et al (2024). (5) Age estimate from soil profiles from Formento-Trigilio and Pazzaglia (1998) for terraces near Walatowa. (6) Age from determination of presence of LCB ash (Rogers, 1996; Pazzaglia et al., 1997; this study). (7) Age estimates for Qt2 from Cron (2012) and Rogers (1996). (8) Nasholds and Zimmerer (2022) age of Tshirege member of the Bandelier Tuff refining the age of Qg3 determined by Rogers (1996). (9) Minimum age from Jean et al. (2024) U-series model age on capping micrite. (10) Nasholds and Zimmerer (2022) age of Otowi member of the Bandelier Tuff. (11)Age from correlation with LCB ash-containing terraces from Rogers (1996) by Pazzaglia et al. (1997). (12) Age estimate from soil profiles taken near Walatowa for Qt2 terraces by Formento-Trigilio and Pazzaglia (1998). * No age constraints available, see Formento-Trigilio and Pazzaglia (1998).

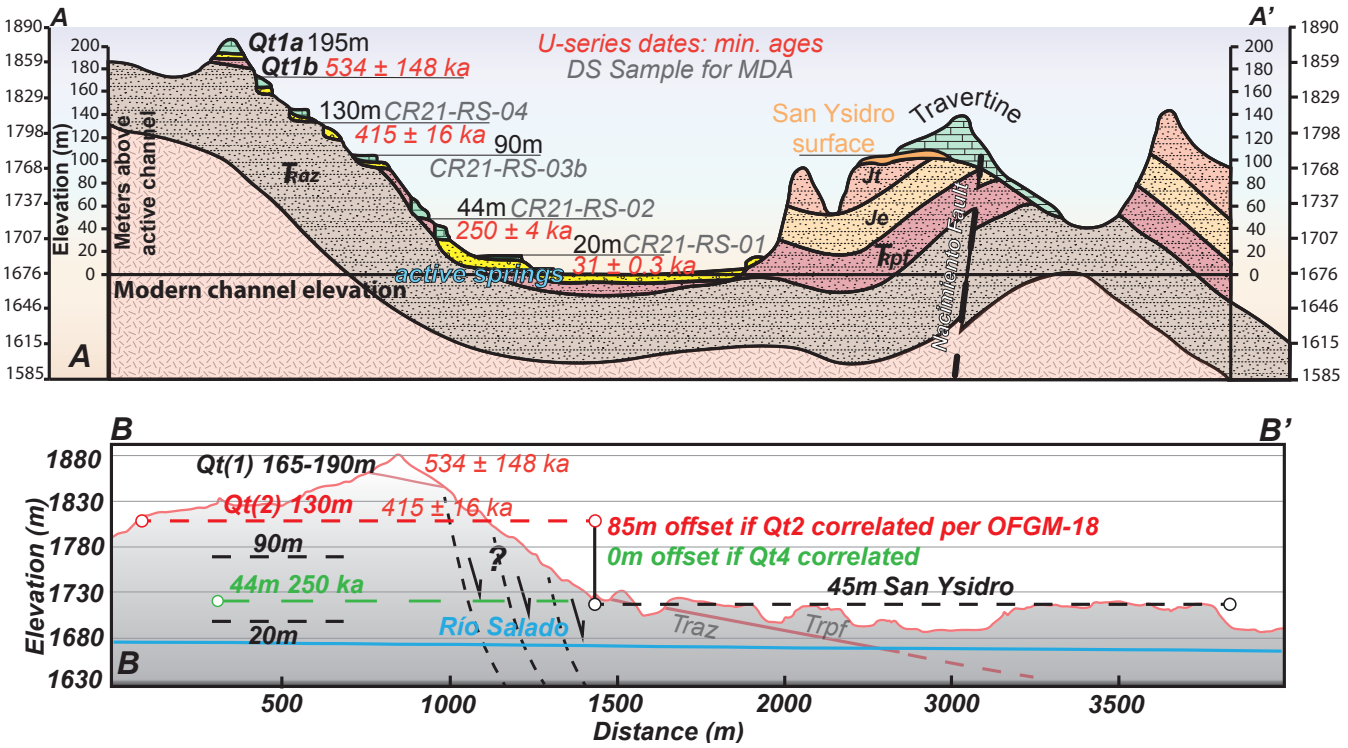

FIGURE 9. (A) Simplified cross section of Rio Salado strath terraces with heights determined with 1m lidar. The Triassic Agua Zarca sandstone forms a S-plunging dip-slope on which the terraces are inset. Ages from U-series dated travertine caps and DS MDAs samples are shown with their respective terrace position. (B) Profile transect of A-A' of Figure 7. Correlated Qt2 terraces are shown between Rio Salado (subarea 2) and San Ysidro (subarea 3) in red (alternative 1) as mapped by Formento-Trigilio et al. (1998). If the published terrace correlation is correct, there is an offset of 85 m across the Towa structure. The alternative 2 correlation is presented in green where terraces in subarea 3 are correlated with Qt4 rather than Qt2; this necessitates no slip across the Towa structure but requires 60 m of the differential incision of Qt2 between subareas 2 and 4 to be accommodated by the San Ysidro and Jemez faults.

Subarea 5 is the upper Rio Jemez near Soda Dam. Terrace correlations between subareas 4 and 5 are complex, as the location is reworked by hydrothermal carbonic springs, extensive travertines, and faults of the Jemez fault system. Frankel and Pazzaglia (2006, fig. 8) correlated the 90-m-ARL Qt1 630 ka terrace of subarea 4 with a 32-m-ARL gravel at Soda Dam and concluded that terraces converge upstream on the Rio Jemez as a response of base-level fall and upstream knickpoint migration. However, Tafoya et al. (2012) and Jean et al. (2024) dated numerous travertine deposits and found that the gravel at 32 m ARL is cemented by 210 ka travertine, making this correlation unlikely, as the difference between depositional age and travertine-cementing age would be ~400 ka in an active travertine setting. Jean et al. (2024) also dated travertine platform A1 that overlies ~150-m-ARL gravels near Soda Dam (Fig. 11). The gravel is intruded by a calcite spar sill of 486±25 ka, which gives a minimum age. Older but still minimum ages are given by imprecise micrite ages from the top of deposit A1 of 755±212 ka (^{238}U model age) and a U-series age of 560±323 ka. We interpret the gravels to have been cemented near the paleoriver bottom as the travertine developed above them, analogous to the modern stream. If so, this would give an incision rate of 268 m/Ma using the strath height, and the oldest reported micrite age that is within U-series range; if the

TABLE 1. Compiled U-series dates on travertines and ^{40}Ar/^{39}Ar DS maximum depositional ages (MDAs) from the Rio Salado terraces. K06-SY-67 is a ^{238}U model age. U-series data is reported in Cron et al. (2024), this volume.

Terrace height	U-series corrected ages (Cron et al., 2024)		^{40}Ar/^{39}Ar DS MDA dates (this study)				
				Latitude	Longitude	Elevation (m)	
20 m	K04-SY-50	31±0.3 ka	CR21-RS-01	35.543187	-106.843635	1695	603±15 ka
40 m	K06-SY-20	250±4 ka	CR21-RS-02	35.545667	-106.841483	1723	20.5±0.3 Ma
90 m			CR21-RS-03b	35.547639	-106.834462	1770	1.08±0.08 Ma
130 m	LC04-SY-5a	415±16 ka	CR21-RS-04	35.552638	-106.83824	1828	1.164±0.01 Ma
195 m	K06-SY-67	534±148 ka	CR21-RS-04	35.552638	-106.83824	1828	1.164±0.01 Ma

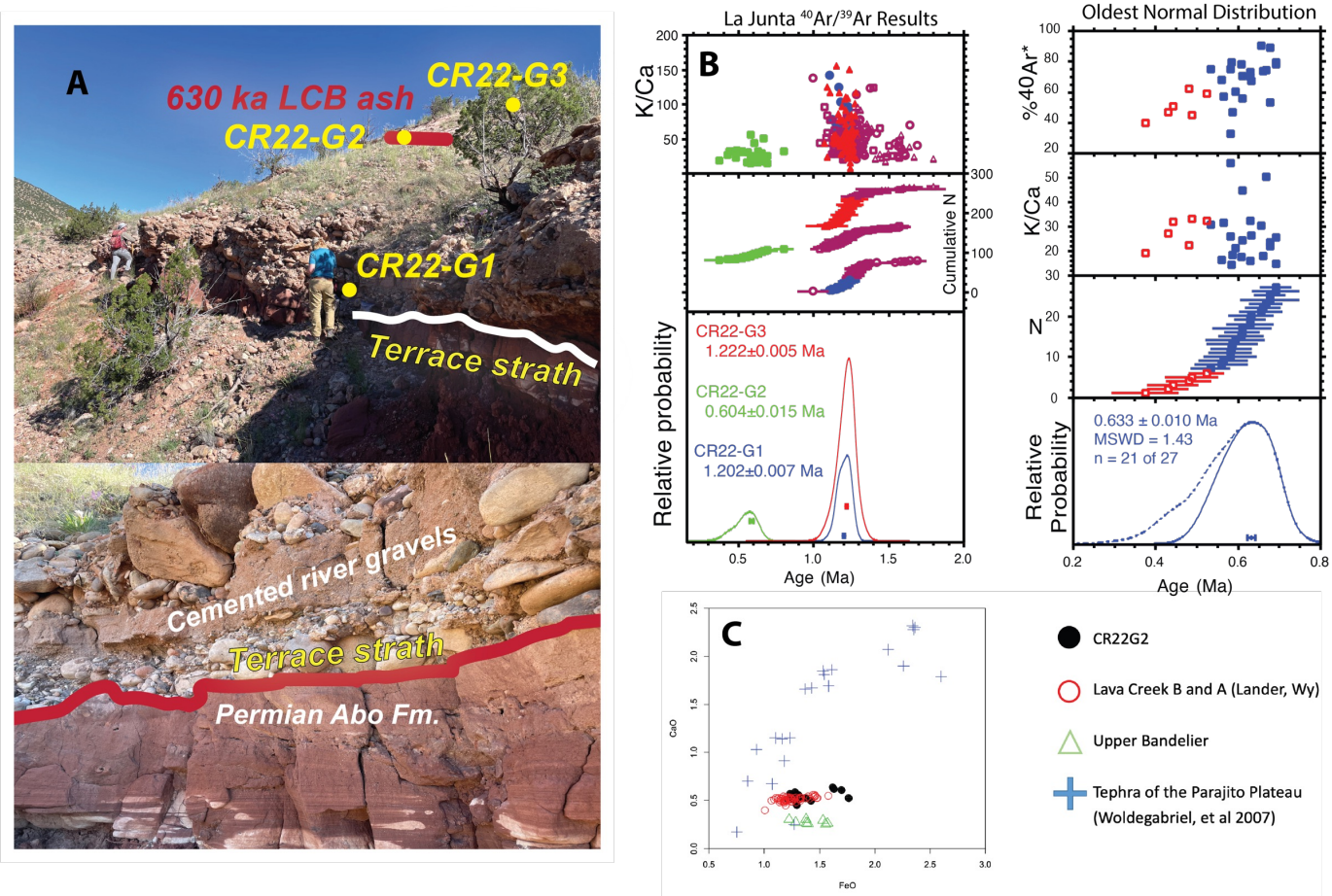

FIGURE 10. (A) Well-exposed bedrock strath cut onto the Abo Formation at base of Qt1 terrace in the La Junta area of subarea 4 (Rogers, 1996; Rogers and Smartt, 1996) and sample locations (yellow) of overlying sands (detrital sanidine and $^{40}Ar/^{39}Ar$ dating) and the Lava Creek B ash (CR22-G2, tephrochronology and $^{40}Ar/^{39}Ar$ dating). (B) $^{40}Ar/^{39}Ar$ geochronology of three samples (CR22-G1, 2, 3) are shown on the left plot. The right plot depicts the distribution of 0.4-0.8 Ma ages for the CR22-G2 sample (direct sample of base of ash). In the right plot, (blue squares denote the older normal distribution of CR22-G2 data. The younger normal distribution (red squares) is rejected because the largest population of data better fit the older distribution. The 604±15 ka combined age and 633 ± 10 ka age for CR22-G2 (from the entire 0.4-0.8 Ma distribution and the older normal distribution of CR22-G2, respectively) are within range of expected LCB ash ages. See Supplementary Data for $^{40}Ar/^{39}Ar$ data. (C) Glass chemistry results from microprobe analysis of sampled material from CR22-G2 supports a match with LCB tephra compared to tephras derived from the nearby late Pleistocene-Pliocene volcanic centers of the Jemez Mountains.

gravels correlate with the Qt1 630 ka terrace from subarea 4, the incision rate would be 238 m/Ma.

Our justifications for interpreting some travertine dates as near-depositional ages for the gravel versus secondary infillings is well-illustrated at Soda Dam, where we have numerous U-series dates. The interpretation of near-primary ages for the 150-m and 32-m gravels is supported by the observation that two younger travertine deposits are inset into Deposit A1. The general age range of micritic ages (not from sills or veins) are younger for progressively lower, inset deposits, as shown in Fig. 8 (e.g., 287–482 ka for A2, 132–183 ka for A3, 78–138 ka for B). The modern setting of travertine-cemented river cobbles at river level provides a good analog for the older micrite deposits. Younger U-series ages of 96–339 ka on sills within deposit A1 are clear examples of secondary travertine infillings due to episodes of high artesian head as the river incised, with high head potentially due to upstream caldera lakes (Jean et al., 2024). These infilling-type deposits can form hundreds of meters above river base level, as also seen in the Tierra Amarilla anticline (Cron et al., 2024), where artesian waters currently move up semiconfined fault conduits.

The proposed 268 m/Ma incision rate at Soda Dam over the past 560 Ma (Fig. 8) is more precise than warranted by the imprecise geochronology, but if we use a range of ages of 560–755 ka, this results in a range of incision rates (199–268 m/Ma) that is ~50–100 m/Ma higher than the 143 m/Ma rate in subarea 4 at La Junta. This is interpreted as due to west-up displacement on the Jemez fault zone. This scale of differential incision is compatible with the ~380-m-ARL height of the base of the 1.62 Ma Otowi Member of the Bandelier Tuff in this area. Using the height and age of the Otowi Member gives a long-term average bedrock incision rate of 235 m/Ma since 1.62 Ma, or 309 m/Ma from the base of the 1.2 Ma Bandelier Tuff (in this area there was little bedrock incision [canyon deepening] between the 1.62 and 1.23 Ma Bandelier Tuff eruptions). These rates are >100 m/Ma higher than those in subarea 4, where the long-term bedrock incision rate has been steady at 140–150 m/Ma since 1.23 Ma based on gravels coeval with

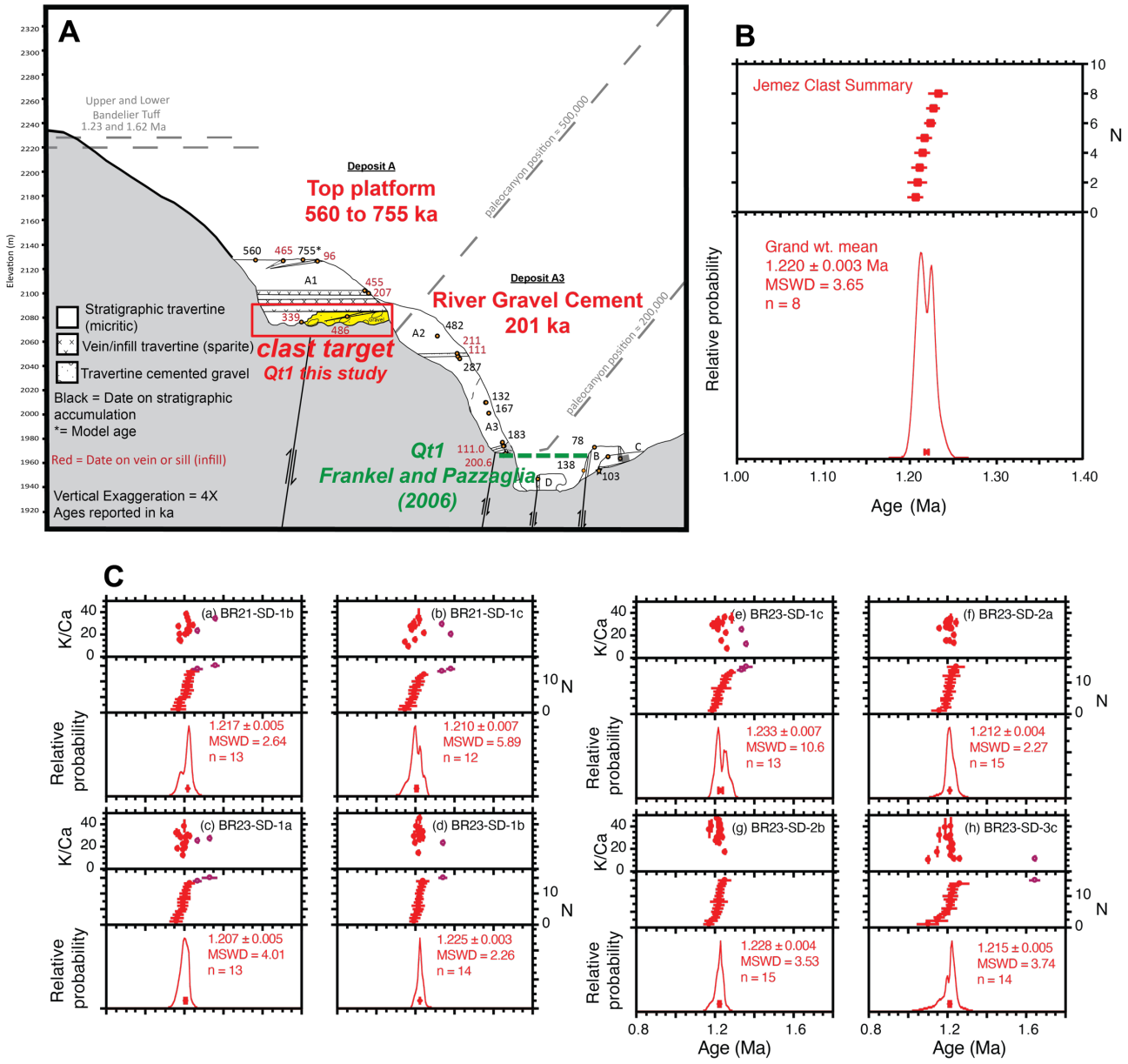

FIGURE 11. (A) Soda Dam travertine ages reported in Tafoya (2012) and Jean et al. (2024).The 150 ARL gravel below deposit A1 is constrained to be older than 560 ka using the younger limit of the micrite at the top of the travertine platform. We sampled rhyolite pebbles in hopes of identifying ~ 550 ka clasts of South Mountain rhyolite and related domes, but all turned out to be Bandelier tuff age (1.22 Ma) with summary ages presented in (B) and individual single grain $^{40}Ar/^{39}Ar$ sanidine analyses for clasts in (C). Other minimum U-series age and the apparent lack of such clasts are consistent with a >550 ka depositional age.

and at the base of the upper Bandelier Tuff (Qg2 and Qg3 of Rogers and Smart, 1996) and based on the 90-m-ARL Qt1 terrace that contains the 0.63 Ma Lava Creek B ash. Correlating the 150-m-ARL Soda Dam gravels with the 90 m/Ma LCB gravels downstream, the associated terrace level (Qt1) appears to diverge upstream (Jean et al., 2024, this volume, their Fig. 10) rather than converge (Frankel and Pazzaglia, 2005), which is compatible with headwater uplift.

DISCUSSION OF DIFFERENTIAL INCISION ACROSS FAULTS

We explore the Formento-Trigilio and Pazzaglia (1996) model that posits that differences in incision relative to correlated terrace straths can be observed across faults and used to estimate fault slip. Formento-Trigilio and Pazzaglia did not consider our subareas 2 and 5 and concluded that fault slip on the Nacimiento and Cross Valley faults was an order of magnitude (13 m/Ma) less then river incision (171 m/Ma). They inferred fault offsets between subareas, but their fault slip rate did not include what we think may be some major Quaternary structures (e.g., the Towa structure), and their river incision rate assumed steady incision across the different areas and did not have the advantage of as extensive a geochronology dataset.

Our discussion of inferred fault vertical offsets is summa-

rized in Figures 7 and 8. We use the highest terrace sets, Qt1 and Qt2. Our preferred correlation for Qt1 from the dated terraces is that the 90-m-ARL, 630 ka, Qt1 LCB terrace in subarea 4 is approximately the same age as the 164-m-ARL, 534±164 ka, Qt1b terrace in subarea 2 and the 150-m-ARL, 500–700 ka, Qt1 gravels at Soda Dam. Even though the analytical error on the U-series model ages in subareas 2 and 5 is large (±150 ka), the ages are compatible with other nearby dates that are within U-series range. The Qt2 terrace correlation relies on earlier mapping and directly tying the ~400 ka age from the travertine in subarea 2 with inferred 400–500 ka age terraces in subarea 4. Both the Qt1 and Qt2 correlations use our assumption that the aforementioned U-series ages of travertine are near-depositional ages.

Using round numbers for the long-term rates to recognize the dating uncertainties, the large height differences in age-similar terraces equates to differential incision along the river system of ~150 m/Ma between subarea 4 (150 m/Ma) and subarea 2 (~ 300 m/Ma) and about 100 m/Ma between subarea 4 (150 m/Ma) and subarea 5 (~250 m/Ma). Given the short distance between areas, the relatively smooth concave-up profiles, low k_{sn} values of the Arroyo Peñasco- Rio Salado-lower Rio Jemez river system (Rogers, 1996; Formento-Trigilio and Pazzaglia, 1998; Frankel and Pazzaglia, 2005), and the known presence of Quaternary faulting, the differential incision is interpreted here to reflect slip on Quaternary faults, with subarea 4 down-dropped relative to subareas 2 and 5. For the ~600 ka terraces (Qt1), we infer up to 75 m of east-down slip between subareas 2 and 4 and 60 m between subareas 4 and 5. Bedrock incision rates were steady back at least to 1.2 Ma in subareas 4 and 5, implying there has been long-lived faulting due to tectonic uplift of the Jemez Mountains and Sierra Nacimiento and/or subsidence of the Rio Grande rift.

More detailed parsing of the Quaternary fault slip on the different structures between the subareas depends on uncertain terrace correlations that require more refined geochronology. Nevertheless, for the major displacements, we infer that ~100 m/Ma of south-down slip has taken place between subareas 4 and 5 across the Jemez fault zone over the past 1.2 Ma. If the published correlations of Qt1 and Qt2 from Formento-Trigilio (1997), Formento-Trigilio et al. (1998), and Formento-Trigilio and Pazzaglia (1998) are correct (Alternative 1), most of the ~85-m offset between subareas 2 and 3 takes place on the enigmatic Towa structure. However, if the subarea 3 terraces correlate with the 250 ka Qt4 instead of the 400 ka Qt2 of subarea 2 (Alternative 2), then slip on the Towa structure was zero or minimal, and the 60 m of differential incision was accommodated by slip was on the San Ysidro and Jemez faults.

Our data between subareas also provide preliminary estimates of differential incision at the tens-of-meters scale (Fig. 8) that hints at the presence of a network of small north-south- and northeast-striking fault segments with distributed Quaternary displacements. Subareas 1 and 2 are not sufficiently well correlated to refine the estimate of Formento-Trigilio and Pazzaglia (1998) of the Quaternary slip on the Nacimiento fault, for which they reported a 17-m-high fault scarp, a knickpoint on the Arroyo Peñasco that coincides with a segment of the Nacimiento fault evidencing young (<250 ka) faulting, and an inferred slip rate of ~10 m/Ma. The Cross Valley fault of Formento-Trigilio and Pazzaglia (1998) cuts between the terraces at San Ysidro (subarea 3) and Walatowa (subarea 4), but the difference in terrace heights can be also explained by east-down displacement on the San Ysidro fault. Comparing differences in terrace heights between subarea 6 (Zia) and subarea 2 (San Ysidro) across the San Ysidro fault reveals 10–15-m-scale differences in heights, depending on how they are correlated, consistent with the 11 m of offset across the San Ysidro-Jemez fault interpreted by Formento-Trigilio and Pazzaglia (1998).

Incision Rates Through Time

There is enough age control on higher surfaces and lower terraces in addition to Qt1 and Qt2 to begin to investigate whether rates were semisteady through time within each terrace sub-area. To do this, we also use the height of Bandelier Tuff units of known age, as shown in Figure 12 for Cañon de San Diego. Cañon de San Diego existed as a canyon before the eruptions of the 1.62 and 1.23 Ma Bandelier Tuffs (Turbeville and Self, 1988; Hulen et al., 1991; Rogers et al., 1996; Kelley et al., 2007) that filled and preserved the pre-eruption topography shown in Figure 12. There are also gravels below the Bandelier Tuffs that preserve a record of pre-1.62 Ma river systems (Rogers, 1996; Smith and Lavine, 1996; Kelley et al., 2007). There was no significant denudation in the San Diego Canyon area between the two eruptions, such that the lower and upper Bandelier Tuff are generally stacked on top of one another in a single cliff (Fig. 12). From the viewpoint of bedrock incision, the tuffs might be considered fill material similar to fill terraces. If so, the height of the base of the 1.62 Ma Otowi Member cliff above the modern Rio Jemez provides a long-term bedrock incision (canyon deepening) rate for Cañon de San Diego (the solid line in Fig. 12A). Considering that the river had to also reincise through ignimbrite fill, the dashed line in Figure 12 reflects incision rates as measured from the top of the 1.23 Bandelier Tuff (Fig. 12B). The dashed line rates are significantly higher than expected because of rivers adjusting to grade following a major perturbation to the landscape (i.e., sudden emplacement of a >100-m-thick ignimbrite).

Near the confluence of the Rio Guadalupe and Rio Jemez (La Junta), Rogers (1996) identified three well-dated buried gravels in the canyon walls. The oldest of these, Qg1, is exposed underneath the 1.62 Ma Otowi Member (LBT) on the sides of Virgin Mesa, Mesa de las Casas, and Guadalupita Mesa approximately 192 m ARL, yielding an estimated incision rate of 119 m/Ma from 1.62 Ma to present. Qg2 is an axial stream gravel that lies approximately 187 m ARL at the southern end of Mesa de Guadalupe and is buried by the basal pumice fall (Tsankawi Pumice) of the 1.23 Ma Tshirege Member (UBT), yielding an incision rate of 152 m/Ma since 1.23 Ma. Qg3, an axial gravel buried directly beneath the Tsankawi pumice, approximately 176 m ARL, was interpreted to be the actual flowing stream at the time of the 1.23 Ma Tshirege eruption (whereby the Qg2 gravel occupied a paleo-terrace). This channel deposit contains Tsankawi pumice that was be-

ing deposited as cross-bedded fluvial pumice bars in the active channel during the eruption until the stream succumbed to the ash flows of the UBT. Incision near La Junta from the Qg3 exposure provides an incision rate of 143 m/Ma since 1.23 Ma, similar to the 152 m/Ma rate calculated from Qg2 and the same as the post-630 ka rate of 143 m/Ma. We prefer this ~143 m/Ma rate to the 171 m/Ma reported by Formento-Trigilio and Pazzaglia (1998, fig. 5), which was based on a regression line that assumed steady incision between 1.2 and 0.3 Ma, but we agree this subarea records steady rates of bedrock incision since 1.62 Ma. Soda Dam (subarea 5) also shows steady long-term average bedrock incision but at different rates than the 143 m/Ma seen in subarea 4. At Soda Dam rates were 238 m/Ma since 1.62 and ~250 m/Ma, assuming a ~600 ka age for the 150-m-ARL gravels. At Rio Salado, rates were 307–313 m/Ma for both Qt1 and Qt2 (Fig. 8).The apparent semisteady

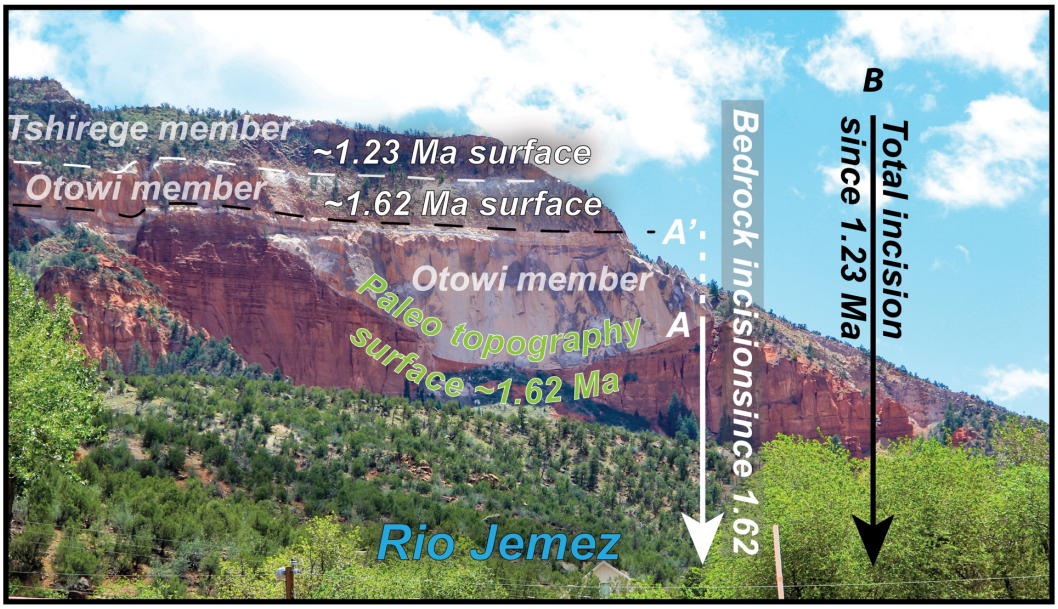

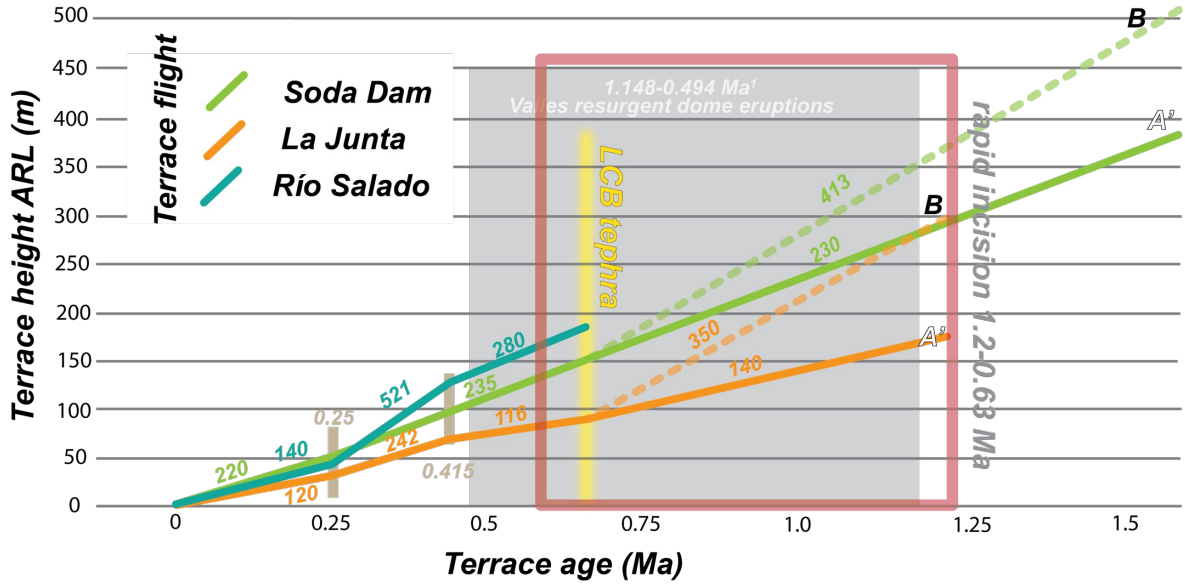

FIGURE 12. Top panel: Paleochannel seen on the east side of Cañon de San Diego (CdSD) preserved just downstream of Soda Dam with different conceptualizations of ways to calculate long terms incision rates. To calculate post-1.62 Ma bedrock incision (canyon deepening): A is height of base of paleochannel above modern river but because the pre-1.62 Ma paleocanyon geometry is incompletely known throughout the canyon, the A' height of base of the 1.62 Ma Otowi Member (base of lowest continuous layer of Otowi = maximum height of underlying paleotopography) or the base of the 1.23 Tshirege Member are generally used as approximations, especially where gravels are present (Rogers and Smartt, 1996). The height of the top of the 1.23 Tshirege Member (B) provides an estimate of the total incision done by the Rio Jemez since 1.23 Ma. Bottom panel: Incision rates through time are shown for three keys terrace flights: subarea 2- Rio Salado on the nose of the Sierra Nacimiento; subarea 4- La Junta; and subarea 5- Soda Dam. Solid line represents bedrock incision using heights (A') from the base of the laterally continuous cliff formed by the Otowi Member; dashed lines (B) represent total incision using the top of the 1.23 Ma Tshirege Member. Use of the base of the cliff (A') in CdSD allows for an approximation of maximum bedrock incision since 1.62 Ma as it does not account for the topographic lows filled in by the Otowi Member.

long-term average bedrock incision rates within these two subareas over the 1.6–0.4 Ma timeframe is consistent with broad epeirogenic uplift of the Jemez Mountains region rather than headward-propagating knickpoints responding to base-level fall (Frankel and Pazzaglia, 2006). Rogers (1996) concluded that incision has been unsteady through time, with low rates (40 m/Ma) between 1.62 and 1.23 Ma, but this was considering the incision that followed emplacement of the Otowi and Tshirege Members compared to young terraces near the modern channel. His reported average for a post-LCB incision rate of ~150 m/Ma used the terrace tread height of 111 m (rather than the 90-m strath height) and an LCB age of 620 ka (rather than 630 ka) but is very similar to our 143 m/Ma rate. Formento-Trigilio and Pazzaglia's (1998) interpretation that average bedrock incision rates were steady at 171 m/Ma based on a regression line through points with significant error bars for both age and height is broadly similar to our 143 m/Ma estimate. They interpreted an increase to short-term rates of 180 m/Ma after their 150 ka Qt4. Because similar rates of differential incision between subareas are seen at 1.62 Ma, 1.23 Ma, and 630 ka timeframes that average out short-term variations, we infer that the difference of 164 and 166 m/Ma for Qt1 between subareas 2 and 5, respectively, and La Junta in subarea 4 seems best interpreted as due to fault-influenced incision.

Figure 12A shows two conceptualizations for calculating long-term rates using the Bandelier Tuffs at Soda Dam and La Junta. The deepest point of paleo Cañon de San Diego is not well exposed, but preserved paleochannel remnants are tens of meters deep (A in Fig. 12A), such that this amount could be (but is usually not) applied to the calculation that uses the well-exposed base of the 1.62 Ma Otowi and 1.23 Tshirege Members as regional surfaces (A' in Fig. 12A). The solid lines in Figure 12B plot bedrock incision (the A' method) and consider the tuffs to be like "fill terraces" that are not included when strath heights are used. The dashed lines plot total incision (the B method) that the river had to accomplish to cut through the tuffs to resume bedrock incision (deepening) of San Diego Canyon. Both curves converge at ~600 ka, the beginning of the terrace record. The result in Figure 12B shows semisteady average rates through time for the past ~600 ka in subareas 4 (La Junta) and 5 (Soda Dam) that are not significantly perturbed by local, accelerated, short-term rates (e.g., after 150 ka; Formento-Trigilio and Pazzaglia, 1998). Long-term bedrock incision rates also remain steady back at least to the 1.2 Ma timescale at La Junta (subarea 4) and Soda Dam (subarea 5). Thus, the key observation from Figure 12B is that long-term average bedrock incision rates are steady within each reach, but they are different from reach to reach.

Caveats and Limitations of Terrace Correlations and Ages

Limitations of most terrace studies include incomplete terrace age data and incomplete preservation that make terrace correlations difficult. Here, we have relied on and refined the Formento-Trigilio and Pazzaglia (1998) Qt1 and Qt2 correlations and extended this correlation to include the highest terraces in two new subareas: Rio Salado and Soda Dam. In both areas, the >500 ka "beyond U-series" results for the highest terraces coupled with imprecise δ^{234}U-model ages and constraints from lower terraces within a given subarea are compatible with the notion, but not definitive, that our highest terraces in each area may be similar in age to the 630 ka Qt1 terrace at La Junta. Our age of 415 ka for Qt2 terraces is compatible with that of prior workers who estimated a ~400 ka age based on other techniques (Rogers and Smartt, 1996; Rogers, 1996; Formento-Trigilio and Pazzaglia, 1998). This correlation leads to our proposed Quaternary fault offsets, but better ages across multiple flights of terraces are needed to continue to test this idea using U-Pb luminescence (IRSL) dating (Nelson et al., 2015; Mahan et al., 2022) and detrital sanidine. Uncertainties near the Rio Salado motivate us to consider two possible end-member correlations. Alternative 1 uses previous mapping (Formento-Trigilio et al., 1998; Formento-Trigilio and Pazzaglia, 1998) and results in 85 m of offset along the Towa structure, along which previous mapping has not identified a notable fault. Alternative 2 correlates terraces between subareas 2 and 3 based solely on terrace heights, resulting in no discernable offset along the Towa structure but allowing tens of meters of throw along the San Ysidro and Jemez faults. A further alternative would be correlating the 45-m-ARL terrace in subarea 3 with the 90-m terrace in subarea 2, allowing 45 m of offset of the Towa structure and a similar amount on the San Ysidro-Jemez structure.

Estimating how closely a geochronologic age from a terrace fill approximates the age of the underlying bedrock strath has uncertainties in all river terrace incision studies, even for terraces containing Lava Creek B ash. It is often assumed that terrace fills closely follow straths during ~100 ka aggradation/incision climate oscillations and river response (Pazzaglia, 2013). In our study, we make a similar assumption that micritic travertine ages (excluding sills or veins) closely postdate deposition of the terrace fill based on various arguments, including analogy to still-active travertine systems. Alternative terrace correlations are important to consider to decipher finer details of differential incision and parsing the inferred fault slip to different fault segments. Additionally, the role of dipping bedrock and bedrock erodibility (Darling et al., 2020; Mitchell and Yanites, 2021) needs to be further investigated as a contributing component for the high incision rates at Rio Salado and Soda Dam relative to the La Junta confluence area.

CONCLUSIONS

The conclusion of this paper is that bedrock incision rate data for the Jemez River system at the 0.4 to 1.6 Ma timescale provide a convincing case that there was overall steady incision history within each reach, whereas bedrock incision differed by ~100 m/Ma between reaches because of displacement on faults. This is based on the two highest mapped terraces in each of six areas of intact terrace flights that are preserved "around the corner" from the west side of the Nacimiento fault on the Arroyo Peñasco, along the Rio Salado, and up the Rio Jemez from San Ysidro to Soda Dam on the Jemez fault zone. New U-series geochronology shows that the uppermost terrac-

es (Qt1) in Rio Salado terrace flight (subarea 2) and near Soda Dam (subarea 5) are both outside of U-series range (>500 ka) but give δ^{234}U-model ages of 465–755 ka and hence are permissively correlated with the Lava Creek B ash (630 ka) Qt1 terrace near the confluence of the Rio Jemez and Rio Guadalupe (subarea 4). Our preferred correlation of the underlying terrace Qt2 is based on relating a U-series age of 415 ka at Rio Salado with ~400 ka age estimates from soil profiles of Qt2 (Formento-Trigilio, 1997) from the confluence area.

If these correlations are correct, the Qt1 and Qt2 straths can be used in tandem to infer different incision rates in the different subareas. This equates to differential incision rates of ~100–150 m/Ma along the river system: ~150 m/Ma between subareas 2 and 4 and ~ 100 m/Ma between subareas 4 and 5. Given the short distances between the areas, the relatively smooth concave-up profiles of both the Rio Salado and Rio Jemez, and the known presence of Quaternary faulting, this differential incision is interpreted to reflect slip on Quaternary faults. If so, subarea 4 has been down-dropped relative to subareas 2 and 5. For the ~600 ka timeframe, ~74 m of east-down slip occurred between subareas 2 and 4 and ~60 m between subareas 4 and 5. We acknowledge other possible correlations, which would change how slip rates are attributed to different faults.

Proposed tectonic influences on river evolution include fault-influenced incision, where upthrown blocks have higher incision rates than downthrown blocks and where the difference is interpreted to be due mainly to fault displacement. If so, the inferred rates of Quaternary fault displacement are ~160 m/Ma between subareas 2 and 4 over the past ~600 ka and hence are similar in magnitude to river incision rates, suggesting that the block uplift has a significant influence on river incision. The faulting itself may be related to rift extension and a broader scale of epeirogenic surface uplift of the combined Sierra Nacimiento-Jemez Mountain areas. The latter is suggested by topographic analysis and by our interpreted upstream-diverging terraces on the Rio Jemez, which indicate that headwater uplift may be interacting with base-level fall in the Rio Grande system at the million-year timescale. Improved terrace geochronology is needed to improve assessment of the magnitude of Quaternary fault displacements in what appears to be a distributed fault network that is elevating the Sierra Nacimiento and Jemez Mountains blocks relative to the adjacent Colorado Plateau and Rio Grande rift provinces.

ACKNOWLEDGMENTS

This work was funded by student research grants to Cameron Reed from the New Mexico Geologic Society, the Geological Society of America, and the Colorado Scientific Society. Matt Heizler and Julia Ricci helped with Ar geochronology and lab analyses. Nels Iverson performed microprobe analyses of La Junta samples. Ben Rodriguez helped with geochronology lab prep and field work and was funded through the New Mexico Alliance for Minority Participation and Leonard Scholarship through the University of New Mexico Department of Earth and Planetary Sciences. The paper was improved by reviews from John Rogers, Fred Phillips, and Dan Koning.

REFERENCES

Aldrich, M.J., 1986, Tectonics of the Jemez lineament in the Jemez Mountains and Rio Grande Rift (USA): Journal of Geophysical Research, v. 91, p. 1753–1762, https://doi.org/10.1029/JB091iB02p01753

Anderson, J.C., Karlstrom, K.E., and Heizler, M.T., 2021, Neogene drainage reversal and Colorado Plateau uplift in the Salt River area, Arizona, USA: Geomorphology, v. 395, 107964, https://doi.org/10.1016/j.geomorph.2021.107964

Armstrong, I.P., Yanites, B.J., Mitchell, N., DeLisle, C., and Douglas, B.J., 2021, Quantifying normal fault evolution from river profile analysis in the northern basin and range province, southwest Montana, USA: Lithosphere, v. 2021, 7866219, https://doi.org/10.2113/2021/7866219

Aslan, A., Karlstrom, K.E., Kirby, E., Heizler, M., Granger, D.E., Feathers, J.K., Hanson, P.R., and Mahan, S.A., 2019, Resolving time-space histories of Late Cenozoic bedrock incision along the Upper Colorado River, USA: Geomorphology, v. 347.

Bridgland, D., and Westaway, R., 2008, Climatically controlled river terrace staircases: A worldwide Quaternary phenomenon: Geomorphology, v. 98, no. 3–4, p. 285–315.

Bull, W.B., 1991, Geomorphic responses to climatic change: Oxford, UK, Oxford University Press.

Bailey, J.M., Karlstrom, K.E., Reed C., and Heizler, M.T., 2024, Structural geology of the Tierra Amarilla anticline, New Mexico, *in* Karlstrom, K.E., Koning, D.J., Lucas, S.G., Iverson, N.A., Crumpler, L.S., Aubele, J.C., Blake, J.M., Goff, F., and Kelley, S.A., eds., Geology of the Nacimiento Mountains and Rio Puerco Valley: New Mexico Geological Society Guidebook 74 (this volume), p. 281–289.

Cather, S.M., Chapin, C.E., and Kelley, S.A., 2012, Diachronous episodes of Cenozoic erosion in southwestern North America and their relationship to surface uplift, paleoclimate, paleodrainage, and paleoaltimetry: Geosphere, v. 8, p. 1177–1206, https://doi.org/10.1130/GES00801.1

Channer, M.A., Ricketts, J.W., Zimmerer, M., Heizler, M., and Karlstrom, K.E., 2015, Surface uplift above the Jemez mantle anomaly in the past 4 Ma based on ^{40}Ar/^{39}Ar dated paleoprofiles of the Rio San Jose, New Mexico, USA: Geosphere, v. 11, p. 1384–1400, https://doi.org/10.1130/GES01145.1

Chapin, C.E., Wilks, M., McIntosh, W.C., 2004, Space-time patterns of Late-Cretaceous to present magmatism in New Mexico—Comparison with Andean volcanism and potential for future volcanism, *in* Cather, S.M., McIntosh, W.A., Kelley, S.A., eds., Tectonics, Geochronology, and Volcanism in the Southern Rocky Mountains and the Rio Grande Rift: New Mexico Bureau of Geology and Mineral Resources Bulletin 160, p. 13–40.

Cikoski, C.T., and Koning, D.J., 2017, Deep-seated landslide susceptibility map of New Mexico: New Mexico Bureau of Geology and Mineral Resources Open-File Report 594.

Cron, B., 2012, Geochemical characteristics and microbial diversity of CO_2-rich mound springs of the Tierra Amarilla anticline, New Mexico [M.S. thesis]: Albuquerque, University of New Mexico, 110 p.

Cron, B., Crossey, L.C., Karlstrom, K.E., Polyak, V., Asmerom, Y., and McGibbon, C, 2024, Geochemistry and microbial diversity of CO_2-rich springs and U-series dating of travertine from the Tierra Amarilla anticline, New Mexico: *in* Karlstrom, K.E., Koning, D.J., Lucas, S.G., Iverson, N.A., Crumpler, L.S., Aubele, J.C., Blake, J.M., Goff, F., and Kelley, S.A., eds., Geology of the Nacimiento Mountains and Rio Puerco Valley: New Mexico Geological Society Guidebook 74 (this volume), p. 225–235.

Crow, R., Karlstrom, K., Darling, A., Crossey, L., Polyak, V., Granger, D., Asmerom, Y., and Schmandt, B., 2014, Steady incision of Grand Canyon at the million year timeframe: A case for mantle-driven differential uplift: Earth and Planetary Science Letters, v. 397, p. 159–173, https://doi.org/10.1016/j.epsl.2014.04.020

Darling, A., Whipple, K., Bierman, P., Clarke, B., and Heimsath, A., 2020, Resistant rock layers amplify cosmogenically-determined erosion rates: Earth Surface Processes and Landforms, v. 45, no. 2, p. 312–330, https://doi.org/10.1002/esp.4730

Dethier, D.P., 2001, Pleistocene incision rates in the western United States calibrated using Lava Creek B tephra: Geology, v. 29, p. 783, https://doi.org/10.1130/0091-7613(2001)029<0783:PIRITW>2.0.CO;2

Formento-Trigilio, M. L., 1997, Soil-landscape relationships in the Jemez River drainage basin, northern New Mexico [unpublished M.S. thesis]: Albuquerque, University of New Mexico.

Formento-Trigilio, M.L., and Pazzaglia, F.J., 1998, Tectonic geomorphology of the Sierra Nacimiento: Traditional and new techniques in assessing long-term landscape evolution in the Southern Rocky Mountains 1: The Journal of Geology, v. 106, p. 433–453, https://doi.org/10.1086/516034

Formento-Trigilio, M., Toya, C., and Pazzaglia, F., 1998, Preliminary geologic map of the San Ysidro quadrangle, Sandoval County, New Mexico: New Mexico Bureau of Geology and Mineral Resources Open-File Geologic Map 18, https://doi.org/10.58799/OF-GM-18

Frankel, K.L., and Pazzaglia, F.J., 2006, Mountain fronts, base-level fall, and landscape evolution: Insights from the southern Rocky Mountains, *in* Willett, S.D., Hovius, N., Brandon, M.T., and Fisher, D.M. eds., Tectonics, Climate, and Landscape Evolution: Geological Society of America, v. 398, https://doi.org/10.1130/2006.2398(26)

Gallen, S.F., and Wegmann, K.W., 2017, River profile response to normal fault growth and linkage: An example from the Hellenic forearc of south-central Crete, Greece: Earth Surface Dynamics, v. 5, p. 161–186, https://doi.org/10.5194/esurf-5-161-2017

Heizler, M.T., Karlstrom, K.E., Albonico, M., Hereford, R., Beard, L.S., Cather, S.M., Crossey, L.J., and Sundell, K.E., 2021, Detrital sanidine $^{40}Ar/^{39}Ar$ dating confirms <2 Ma age of Crooked Ridge paleoriver and subsequent deep denudation of the southwestern Colorado Plateau: Geosphere, v. 17, p. 438–454, https://doi.org/10.1130/GES02319.1

Hobson, R.D., 1972, Surface roughness in topography: Quantitative approach, *in* Chorley, R.J., ed., Spatial Analysis in Geomorphology (first edition): Routledge, p. 221–246.

Howard, A.D., Dietrich, W.E., and Seidl, M.A., 1994, Modeling fluvial erosion on regional to continental scales: Journal of Geophysical Research: Solid Earth, v. 99, p. 13971–13986, https://doi.org/10.1029/94JB00744

Hulen, J.B., Nielson, D.L., and Little, T.M., 1991, Evolution of the western Valles Caldera complex, New Mexico: Evidence from intracaldera sandstones, breccias, and surge deposits, Journal of Geophysical Research, v. 96, no. B5, p. 8127–8142, https://doi.org/10.1029/91JB00374

Jaiswara, N.K., Kotluri, S.K., Pandey, P., and Pandey, A.K., 2020, MATLAB functions for extracting hypsometry, stream-length gradient index, steepness index, chi gradient of channel and swath profiles from digital elevation model (DEM) and other spatial data for landscape characterisation: Applied Computing and Geosciences, v. 7, 100033, https://doi.org/10.1016/j.acags.2020.100033

Jean, A., Crossey, L.J., Karlstrom, K.E., Polyak, V., and Asmerom, Y., 2024, Uranium-series geochronology of travertine from Soda Dam, New Mexico: A Quaternary record of episodic spring discharge and river incision in the Jemez Mountains, *in* Karlstrom, K.E., Koning, D.J., Lucas, S.G., Iverson, N.A., Crumpler, L.S., Aubele, J.C., Blake, J.M., Goff, F., and Kelley, S.A., eds., Geology of the Nacimiento Mountains and Rio Puerco Valley: New Mexico Geological Society Guidebook 74 (this volume), p. 257–270.

Jicha, B.R., Singer, B.S., and Sobol, P., 2016, Re-evaluation of the ages of $^{40}Ar/^{39}Ar$ sanidine standards and supereruptions in the western U.S. using a Noblesse multi-collector mass spectrometer: Chemical Geology, v. 431, p. 54–66, https://doi.org/10.1016/j.chemgeo.2016.03.024

Karlstrom, K.E., Crow, R.S., Peters, L., McIntosh, W., Raucci, J., Crossey, L.J., Umhoefer, P., and Dunbar, N., 2007, $^{40}Ar/^{39}Ar$ and field studies of Quaternary basalts in Grand Canyon and model for carving Grand Canyon: Quantifying the interaction of river incision and normal faulting across the western edge of the Colorado Plateau: Geological Society of America Bulletin, v. 119, p. 1283–1312, https://doi.org/10.1130/0016-7606(2007)119[1283:AAFSOQ]2.0.CO;2

Karlstrom, K.E., Crow, R., Crossey, L.J., Coblentz, D., and Wijk, J.W.V., 2008, Model for tectonically driven incision of the younger than 6 Ma Grand Canyon: Geology, v. 36, p. 835–838, https://doi.org/10.1130/G25032A.1

Karlstrom, K.E., et al., 2012, Mantle-driven dynamic uplift of the Rocky Mountains and Colorado Plateau and its surface response: Toward a unified hypothesis: Lithosphere, v. 4, p. 3–22, https://doi.org/10.1130/L150.1

Karlstrom, K.E., Crossey, L.J., Embid, E., Crow, R., Heizler, M., Hereford, R., Beard, L.S., Ricketts, J.W., Cather, S., and Kelley, S., 2016, Cenozoic incision history of the Little Colorado River: Its role in carving Grand Canyon and onset of rapid incision in the past ca. 2 Ma in the Colorado River System: Geosphere, v. 13, p. 49–81, doi:10.1130/GES01304.1

Karlstrom, K.E., Koning, D., Lucas, S.G., Crumpler, L.S., Goff, F., Kelley, S., Iverson, N., Reed, C., and Crossey, L.J., 2024, Synopsis of the Nacimiento geologic nexus, *in* Karlstrom, K.E., Koning, D.J., Lucas, S.G., Iverson, N.A., Crumpler, L.S., Aubele, J.C., Blake, J.M., Goff, F., and Kelley, S.A., eds., Geology of the Nacimiento Mountains and Rio Puerco Valley: New Mexico Geological Society Guidebook 74 (this volume), p. 105–126.

Kelley, S.A., Osburn, R.G., and Kempter, K.A., 2007, Geology of Canon de San Diego, southwestern Jemez Mountains, north-central New Mexico, *in* Kues, B.S., Kelley, S.A., and Lueth, V.W., eds., Geology of the Jemez Region II: Geology of the Jemez Region II, New Mexico Geological Society Guidebook 58, p. 169–181, https://doi.org/10.56577/FFC-58.169

Kelley, S.A., et al., 2023, Geologic map of the Los Alamos 30 x 60-Minute quadrangle, 1: 24,000 scale compilation of the Los Alamos, Rio Arriba, Santa Fe, and Sandoval Counties, New Mexico: New Mexico Bureau of Geology and Mineral Resources Open-File Geologic Map 298.

Kelley, V.C., 1977, Geology of Albuquerque basin, New Mexico: New Mexico Bureau of Mines and Mineral Resources Memoir 33, 59 p., https://doi.org/10.58799/M-33

Kelson, K.I., Personius, S.F., Haller, K.M., Koning, D.J., and Jochems, A.P., compilers, 2015, Fault number 2029b, Jemez-San Ysidro fault, San Ysidro section, *in* Quaternary fault and fold database of the United States: U.S. Geological Survey, https://earthquakes.usgs.gov/hazards/qfaults, accessed May 10, 2024.

Kirby, E., and Whipple, K.X., 2012, Expression of active tectonics in erosional landscapes: Journal of Structural Geology, v. 44, p. 54–75, https://doi.org/10.1016/j.jsg.2012.07.009

Love, D.W., Connell, S.D., and Lucas, S., 2005, Late Neogene drainage developments on the southeastern Colorado Plateau, New Mexico: New Mexico Museum of Natural History and Science Bulletin, v. 28, p. 151–169.

Magnani, M.B., Miller, K.C., Levander, A., and Karlstrom, K., 2004, The Yavapai-Mazatzal boundary: A long-lived tectonic element in the lithosphere of southwestern North America: Geological Society of America Bulletin, v. 116, p. 1137–1142, https://doi.org/10.1130/B25414.1

McCalpin, J.P., Harrison, J.B.J., Berger, G.W., and Tobin, H.C., 2011, Paleoseismicity of a low slip-rate normal fault in the Rio Grande rift, USA: The Calabacillas fault, Albuquerque, New Mexico, *in* Audemard, F.A.A., Michetti, A.M., and McCalpin, J.P., eds., Geological Criteria for Evaluating Seismicity Revisited: Forty Years of Paleoseismic Investigations and the Natural Record of Past Earthquakes: Geological Society of America Special Papers, v. 479, https://doi.org/10.1130/SPE479

Mitchell, N.A., and Yanites, B.J., 2021, Bedrock river erosion through dipping layered rocks: Quantifying erodibility through kinematic wave speed: Earth Surface Dynamics, v. 9, p. 723–753, https://doi.org/0.5194/esurf-9-723-2021

Nasholds, M.W.M., and Zimmerer, M.J., 2022, High-precision $^{40}Ar/^{39}Ar$ geochronology and volumetric investigation of volcanism and resurgence following eruption of the Tshirege Member, Bandelier Tuff, at the Valles Caldera: Journal of Volcanology and Geothermal Research, v. 431, 107624, https://doi.org/10.1016/j.jvolgeores.2022.107624

Nelson, M.S., Gray, H.J., Johnson, J.A., Rittenour, T.M., Feathers, J.K., and Mahan, S.A., 2015, User guide for luminescence sampling in archaeological and geological contexts: Advances in Archaeological Practice, v. 3, no. 2, p. 166–177, https://doi.org/10.7183/2326-3768.3.2.166

Nereson, A., Stroud, J., Karlstrom, K., Heizler, M., and McIntosh, W., 2013, Dynamic topography of the western Great Plains: Geomorphic and $^{40}Ar/^{39}Ar$ evidence for mantle-driven uplift associated with the Jemez lineament of NE New Mexico and SE Colorado: Geosphere, v. 9, p. 521–545, https://doi.org/10.1130/GES00837.1

Ohmori, H., 1993, Changes in the hypsometric curve through mountain building resulting from concurrent tectonics and denudation: Geomorphology, v. 8, p. 263–277, https://doi.org/10.1016/0169-555X(93)90023-U

Pazzaglia, F.J., 2013, Fluvial terraces, *in* Wohl, E., ed., Treatise of Geomorphology: Amsterdam, Elsevier.

Pazzaglia, F.J., Pederson, J.L., Garcia, A.F., Koning, D.J., Formento-Trigilio, M.L., and Toya, C., 1997, Geologic map of the Jemez Pueblo quadrangle, Sandoval County, New Mexico: New Mexico Bureau of Geology and Mineral Resources Open-File Digital Geologic Map 014, scale 1:24,000.

Pederson, J., Karlstrom, K., Sharp, W., and McIntosh, W., 2002, Differential incision of the Grand Canyon related to Quaternary faulting—Constraints from U-series and Ar/Ar dating: Geology, v. 30, p. 739–742, https://doi.org/10.1130/0091-7613(2002)030<0739:DIOTGC>2.0.CO;2

Perkins, M.E., Nash, W.P., Brown, F.H., and Fleck, R.J., 1995, Fallout tuffs of Trapper Creek, Idaho—A record of Miocene explosive volcanism in the Snake River Plain volcanic province: Geological Society of America Bulletin, v. 107, p. 1484–1506, https://doi.org/10.1130/0016-7606(1995)107<1484:FTOTCI>2.3.CO;2

Perron, J.T., and Royden, L., 2013, An integral approach to bedrock river profile analysis: Integral approach to river profile analysis: Earth Surface Processes and Landforms, v. 38, p. 570–576, https://doi.org/10.1002/esp.3302

Pike, R.J., and Wilson, S.E., 1971, Elevation-relief ratio, hypsometric integral, and geomorphic area-altitude analysis: Geological Society of America Bulletin, v. 82, p. 1079–1084.

Purinton, B., and Bookhagen, B., 2017, Validation of digital elevation models (DEMs) and comparison of geomorphic metrics on the southern Central Andean Plateau: Earth Surface Dynamics, v. 5, p. 211–237, https://doi.org/10.5194/esurf-5-211-2017

Repasch, M., Karlstrom, K., Heizler, M., and Pecha, M., 2017, Birth and evolution of the Rio Grande fluvial system in the past 8 Ma: Progressive downward integration and the influence of tectonics, volcanism, and climate: Earth-Science Reviews, v. 168, p. 113–164, https://doi.org/10.1016/j.earscirev.2017.03.003

Riley, S.J., DeGloria, S.D., and Elliot, R., 1999, Index that quantifies topographic heterogeneity: Intermountain Journal of Sciences, v. 5, p. 23–27.

Ritter, D.F., Kochel, R.C., Miller, J.R., and Miller, J.R., 2002, Process Geomorphology (third edition): Dubuque, IA, William C. Brown, 546 p.

Rogers, J.B., 1996, The fluvial landscape evolution of San Diego Canyon, Jemez Mountains, New Mexico [unpublished M.S. thesis]: Albuquerque, University of New Mexico.

Rogers, J.B. and Smartt, R.A., 1996, Climatic influences on Quaternary alluvial stratigraphy and terrace formation in the Jemez River valley, New Mexico, *in* Goff, F., Kues, B.S., Rogers, M.A., McFadden, L.D., and Gardner, J.N., eds., Jemez Mountains Region: New Mexico Geological Society Guidebook 47, https://doi.org/10.56577/FFC-47.347

Rogers, J., Smith, G.A., and Rowe, H., 1996, History of formation and drainage of Pleistocene lakes in the Valles Caldera, *in* Goff, F., Kues, B.S., Rogers, M.A., McFadden, L.D., and Gardner, J.N., eds., Jemez Mountains Region: New Mexico Geological Society Guidebook 47, p. 14–16, https://doi.org/10.56577/FFC-47

Schwanghart, W., and Scherler, D., 2014, Short Communication: TopoToolbox 2 – MATLAB-based software for topographic analysis and modeling in Earth surface sciences: Earth Surface Dynamics, v. 2, p. 1–7, https://doi.org/10.5194/esurf-2-1-2014

Sklar, L., and Dietrich, W.E., 1998, River longitudinal profiles and bedrock incision models: Stream power and the influence of sediment supply: American Geophysical Union Geophysical Monograph, v. 107, p. 237–260.

Smith, G.A., and Lavine, A., 1996, What is the Cochiti Formation?, *in* Goff, F., Kues, B.S., Rogers, M.A., McFadden, L.D., and Gardner, J.N., eds., Jemez Mountains Region: New Mexico Geological Society Guidebook 47, p. 219–224, https://doi.org/10.56577/FFC-47.219

Strahler, A.N., 1952, Hypsometric (area-altitude) analysis of erosional topography: Geological Society of America Bulletin, v. 63, p. 1117–1142, https://doi.org/10.1130/0016-7606(1952)63[1117:HAAOET]2.0.CO;2

Tafoya, A.J., 2012, Uranium-series geochronology and stable isotope analysis of travertine from Soda Dam, New Mexico: A Quaternary record of episodic spring discharge and river incision in the Jemez Mountains hydrothermal system [M.S. thesis]: Albuquerque, University of New Mexico, 113 p., https://digitalrepository.unm.edu/eps_etds/87

Thompson Jobe, J.A., and Chupik, C., 2021, Low-rate faulting on the margin of the Colorado Plateau and Rio Grande rift in north-central New Mexico: Tectonics, v. 40, e2021TC006860, https://doi.org/10.1029/2021TC006860

Tucker, G.E., and Whipple, K.X., 2002, Topographic outcomes predicted by stream erosion models: Sensitivity analysis and intermodel comparison: Journal of Geophysical Research: Solid Earth, v. 107, no. B9, p. ETG 1-1–ETG 1-16, https://doi.org/10.1029/2001jb000162

Turbeville, B.N., and Self, S., 1988, San Diego Canyon ignimbrites: Pre-Bandelier tuff explosive rhyolitic volcanism in the Jemez Mountains, New Mexico: Journal of Geophysical Research, v. 93, no. B6, p. 6148–6156, https://doi.org/10.1029/JB093iB06p06148

U.S. Geological Survey, 2019, National hydrography dataset (version: National Hydrography Dataset Best Resolution [NHD] for Hydrologic Unit [HU] 4 – 2024, published 20191002), https://www.usgs.gov/national-hydrography/access-national-hydrography-products

U.S. Geological Survey, n.d., Quaternary fault and fold database of the United States, https://www.usgs.gov/natural-hazards/earthquake-hazards/faults

Wegmann, K.W., and Pazzaglia, F.J., 2009, Late Quaternary fluvial terraces of the Romagna and Marche Apennines, Italy: Climatic, lithologic, and tectonic controls on terrace genesis in an active orogen: Quaternary Science Reviews, v. 28, p. 137–165, https://doi.org/10.1016/j.quascirev.2008.10.006

Whipple, K.X., and Tucker, G.E., 1999, Dynamics of the stream-power river incision model: Implications for height limits of mountain ranges, landscape response timescales, and research needs: Journal of Geophysical Research: Solid Earth, v. 104, p. 17661–17674, https://doi.org/10.1029/1999jb900120

Whipple, K.X., and Tucker, G.E., 2002, Implications of sediment-flux-dependent river incision models for landscape evolution: Journal of Geophysical Research: Solid Earth, v. 107, p. ETG 3-1–ETG 3-20, https://doi.org/10.1029/2000JB000044

Whittaker, A.C., Attal, M., Cowie, P.A., Tucker, G.E., and Roberts, G., 2008, Decoding temporal and spatial patterns of fault uplift using transient river long profiles: Geomorphology, v. 100, p. 506–526, https://doi.org/10.1016/j.geomorph.2008.01.018

Willett, S.D., McCoy, S.W., Perron, J.T., Goren, L., and Chen, C.-Y., 2014, Dynamic reorganization of river basins: Science, v. 343, 1248765, https://doi.org/10.1126/science.1248765

Wisniewski, P.A., and Pazzaglia, F.J., 2002, Epeirogenic controls on Canadian River incision and landscape evolution, Great plains of northeastern New Mexico: The Journal of Geology, v. 110, no. 4, p. 437–456, https://doi.org/10.1086/340441

Wobus, C., Whipple, K.X., Kirby, E., Snyder, N., Johnson, J., Spyropolou, K., Crosby, B., and Sheehan, D., 2006, Tectonics from topography: Procedures, promise, and pitfalls, *in* Willett, S.D., Hovius, N., Brandon, M.T., and Fisher, D.M. eds., Tectonics, Climate, and Landscape Evolution, Geological Society of America Special Papers, v. 398, https://doi.org/10.1130/2006.2398(04)

WoldeGabriel G., Naranjo A.P., Fittipaldo M.M., 2007, Distribution, geochemistry, and correlation of Pliocene tephra in the Pajarito Plateau, *in* Kues, B.S., Kelley, S.A., and Lueth, V.W., eds., Geology of the Jemez Region II: New Mexico Geological Society Guidebook 58, p. 275–283, https://doi.org/10.56577/FFC-58.275

Woodward, L.A., and Reutschilling, 1976, Geology of the San Ysidro quadrangle, New Mexico: New Mexico Bureau of Mines and Mineral Resources Geologic Map 37, scale 1:24,000, https://doi.org/10.58799/GM-37